

# Complete sequencing of a cynomolgus macaque major histocompatibility complex haplotype

Julie A. Karl,<sup>1,3</sup> Trent M. Prall,<sup>1,3</sup> Hailey E. Bussan,<sup>1</sup> Joshua M. Varghese,<sup>1</sup> Aparna Pal,<sup>1</sup> Roger W. Wiseman,<sup>1,2</sup> and David H. O'Connor<sup>1,2</sup>

<sup>1</sup>Department of Pathology and Laboratory Medicine, School of Medicine and Public Health, University of Wisconsin–Madison, Madison, Wisconsin 53705, USA; <sup>2</sup>Wisconsin National Primate Research Center, University of Wisconsin–Madison, Madison, Wisconsin 53715, USA

Macaques provide the most widely used nonhuman primate models for studying the immunology and pathogenesis of human diseases. Although the macaque major histocompatibility complex (MHC) region shares most features with the human leukocyte antigen (HLA) region, macaques have an expanded repertoire of MHC class I genes. Although a chimera of two rhesus macaque MHC haplotypes was first published in 2004, the structural diversity of MHC genomic organization in macaques remains poorly understood owing to a lack of adequate genomic reference sequences. We used ultralong Oxford Nanopore and high-accuracy Pacific Biosciences (PacBio) HiFi sequences to fully assemble the ~5.2-Mb M3 haplotype of an MHC-homozygous, Mauritian-origin cynomolgus macaque (*Macaca fascicularis*). The MHC homozygosity allowed us to assemble a single MHC haplotype unambiguously and avoid chimeric assemblies that hampered previous efforts to characterize this exceptionally complex genomic region in macaques. The high quality of this new assembly is exemplified by the identification of an extended cluster of six *Mafa*–*AG* genes that contains a recent duplication with a highly similar ~48.5-kb block of sequence. The MHC class II region of this M3 haplotype is similar to the previously sequenced rhesus macaque haplotype and HLA class II haplotypes. The MHC class I region, in contrast, contains 13 *MHC-B* genes, four *MHC-A* genes, and three *MHC-E* genes (vs. 19 *MHC-B*, two *MHC-A*, and one *MHC-E* in the previously sequenced haplotype). These results provide an unambiguously assembled single contiguous cynomolgus macaque MHC haplotype with fully curated gene annotations that will inform infectious disease and transplantation research.

[Supplemental material is available for this article.]

Rhesus (*Macaca mulatta*) and cynomolgus (*Macaca fascicularis*) macaques are the most widely used nonhuman primate models for infectious disease and transplantation research (Anderson and Kirk 2013; Burwitz et al. 2017; Knechtle et al. 2019; Shiina and Blancher 2019; D'Souza et al. 2022). Proper utilization of a model organism of human disease requires a deep understanding of the immune system and the genetic determinants that govern its responses. The major histocompatibility complex (MHC) encodes an array of gene products that are critical for host immune responses against infection as well as transplanted cells and tissues (Horton et al. 2004; Trowsdale and Knight 2013; Shiina et al. 2017). The most widely studied of these are the MHC class I (MHC-I) proteins that contain highly polymorphic peptide binding domains that play key roles in adaptive immunity by displaying endogenous antigens on the cell surface for surveillance by CD8<sup>+</sup> cytotoxic T cells. Many MHC-I proteins also play an important role in innate immunity by serving as ligands for missing self receptors on innate lymphocytes (Trowsdale and Knight 2013; Kansler and Li 2019). In contrast, MHC class II (MHC-II) proteins form heterodimers to present exogenous peptides to CD4<sup>+</sup> helper T cells. MHC-II expression is largely confined to a subset of lymphoid cell types, whereas MHC-I proteins are expressed by most tissues. Several additional genes in the MHC-II region encode proteins involved in proteasome processing (*PSMB8*, *PSMB9*) and pep-

tide antigen transport (*TAP1*, *TAP2*, *TAPBP*) (Horton et al. 2004). The MHC class III genomic region, which lies between the MHC-I and MHC-II regions, also encodes several classes of immune proteins, including cytokines (*TNF*, *LTA*, *LTB*) and the complement cascade (*C2*, *C4A*, *C4B*, *CFB*) (Horton et al. 2004).

Genome-wide association studies have implicated more associations between the MHC and human autoimmune, inflammatory, and infectious diseases than any other region of the genome (Horton et al. 2004; Trowsdale and Knight 2013). Although many of these human disease associations have been attributed to specific MHC-I and MHC-II alleles, linkage disequilibrium in this gene-dense region makes the identification of specific causative variants for disease phenotypes extremely challenging. Non-immune system loci that make up the majority of genes in the MHC region are also likely to be responsible for a number of disease associations, so characterizing allelic variation in these genes is also essential for establishing genotype/phenotype correlations.

However, the reference genome sequences for the MHC of macaques remain inaccurate, especially in the MHC-I region. Unlike human leukocyte antigen (HLA) haplotypes, which contain three highly polymorphic class I genes (*HLA-A*, *HLA-B*, and *HLA-C*), the macaque MHC genomic region has undergone complex duplication, deletion, and rearrangement events such that different haplotypes contain a variable number of class I loci (Daza-Vamenta et al.

<sup>3</sup>These authors contributed equally to this work.

Corresponding author: dhoconno@wisc.edu

Article published online before print. Article, supplemental material, and publication date are at <https://www.genome.org/cgi/doi/10.1101/gr.277429.122>.

© 2023 Karl et al. This article is distributed exclusively by Cold Spring Harbor Laboratory Press for the first six months after the full-issue publication date (see <https://genome.cshlp.org/site/misc/terms.xhtml>). After six months, it is available under a Creative Commons License (Attribution-NonCommercial 4.0 International), as described at <http://creativecommons.org/licenses/by-nc/4.0/>.

2004; Fukami-Kobayashi et al. 2005; Shiina et al. 2006; Watanabe et al. 2007). Sequencing of an MHC class I B haplotype from a rhesus macaque bacterial artificial chromosome (BAC) library (CHORI-250) identified 19 distinct *MHC-B* genes (Daza-Vamenta et al. 2004; Shiina et al. 2006). Extensive sequencing of MHC-I transcript and genomic DNA PCR amplicons suggests that this expansion of *MHC-B* genes is common in both rhesus and cynomolgus macaques (Otting et al. 2005; Doxiadis et al. 2013; Wiseman et al. 2013; Karl et al. 2017; Shortreed et al. 2020). These *MHC-B* duplication events appear to have arisen after the divergence of macaques and humans from their most recent common ancestor ~27 Myr ago (Fukami-Kobayashi et al. 2005). Macaques lack a clear ortholog of *HLA-C* that is estimated to have been duplicated from *HLA-B* ~22 Myr ago (Fukami-Kobayashi et al. 2005). Furthermore, transcript sequencing has provided evidence for the existence of multiple *MHC-A* and *MHC-E* genes per individual macaque haplotype (Wu et al. 2018; de Groot et al. 2020). In contrast to humans, macaques have lost a functional nonclassical *MHC-G* gene. The *HLA-G* locus has been replaced by a fusion of *MHC-A* and *MHC-G* genes, referred to as *MHC-AG*, that is expressed in the placenta and contributes to maternal tolerance of fetuses (Boyson et al. 1999). The *MHC-AG* gene regions of both rhesus and cynomolgus macaques have undergone a similar duplication as their classical MHC-I counterparts *MHC-A* and *MHC-B* (Daza-Vamenta et al. 2004; Shiina et al. 2006, 2017).

The implications for macaque MHC-I gene duplication are unclear. It has been established that various *MHC-A* and *MHC-B* genes use differential levels of steady-state RNA that we distinguish with “major” and “minor” allele designations (Otting et al. 2005; Budde et al. 2010; Karl et al. 2013). Relative transcriptional levels of MHC-I genes result in differential cell surface expression (Rosner et al. 2010). Some macaque MHC-I genes are expressed differentially in distinct leukocyte subsets, suggesting the existence of differential function among duplicated genes (Greene et al. 2011). Furthermore, MHC expression is known to vary wildly between tissue subsets (Boegel et al. 2018). Genomic assemblies of multiple MHC region configurations are a prerequisite to understanding the differential functions of these duplicated genes and how macaques manage to balance an expanded repertoire of MHC-I genes without causing autoimmunity.

Because of the importance of macaques in immunological research, thousands of classical and nonclassical class I and class II macaque MHC cDNA transcript sequences have been cataloged (Shiina and Blancher 2019). However, the genomic context of these transcript sequences is largely unexplored. A single Indian rhesus macaque MHC haplotype was sequenced by Daza-Vamenta et al. in 2004 and was resequenced by Shiina et al. in 2006 (Daza-Vamenta et al. 2004; Shiina et al. 2006). In both cases, the overlapping BACs were derived from an MHC-heterozygous macaque, leading to chimeric sequences that do not reflect a single, intact MHC haplotype. Obtaining additional MHC haplotype sequences has been complicated by the high degree of conservation among the closely related, duplicated genes. This difficulty is shown by gaps and artificial sequence mergers in the MHC-I regions of publicly available rhesus (Mmul\_10) and cynomolgus (MFA1912RKSv2) macaque genome reference builds (Warren et al. 2020; Jayakumar et al. 2021).

Sequencing techniques like ultralong Oxford Nanopore Technologies (ONT) sequencing and Pacific Biosciences (PacBio) HiFi circular consensus sequencing are increasingly being applied to resolving genomic regions that were historically difficult to characterize. Ultralong DNA reads spanning repetitive sequence motifs

like segmentally duplicated genes, transposable elements, short tandem repeats, and homopolymer stretches can be unambiguously assembled into chromosome-level scaffolds (Jain et al. 2018; Nurk et al. 2022). Such repetitive elements are abundant within the macaque MHC. The ultralong scaffolds can be combined with higher-accuracy sequencing like PacBio HiFi reads for error correction (Wenger et al. 2019; Nurk et al. 2020). Additional details about ONT and PacBio sequencing and their utility for resolving difficult-to-assemble genomic regions are provided in the [Supplemental Information](#). Applying state-of-the-art sequencing techniques to the macaque MHC region will result in an unprecedented resolution of the genomic architecture.

The genetic diversity of Mauritian-origin cynomolgus macaques (MCMs) is far less than that of other species of macaques with research significance owing to geographic isolation and a founder effect (Sussman and Tattersall 1986). The entire MHC diversity within the MCM population can be characterized by seven ancestral haplotypes that extend from the class I through class II regions. For comparison, we recently described regional haplotypes for 70 *Mafa-A*, 78 *Mafa-B*, and 45 *Mafa-DRB* gene clusters in a single breeding colony of Indonesian-origin cynomolgus macaques (Shortreed et al. 2020). Likewise, earlier studies have described 17–21 *Mamu-A* and 18–30 *Mamu-B* haplotypes in Indian-origin rhesus macaques from several different colonies (Doxiadis et al. 2013; Karl et al. 2013; Wiseman et al. 2013). This unique genetic homogeneity allows for the selection of MHC-homozygous individuals with relative ease. For the current study, we sequenced an animal that is homozygous for the M3 MHC haplotype. This M3 haplotype is the second most abundant ancestral haplotype in the MCM population, accounting for 14% of the MHC haplotypes overall (Wiseman et al. 2013). Furthermore, cDNA allelic transcripts are fully characterized for most of the variable MHC classical class I and class II genes, allowing us to estimate the error rate of genomic assemblies accurately.

Here we take advantage of the strengths of ONT and PacBio HiFi sequencing to generate an approximately 60× ONT and approximately 30× PacBio HiFi coverage genome of an MHC-homozygous MCM, creating the most complete macaque MHC sequence to date. This full genomic MHC region assembly provides an important new comparator for understanding differences between macaque and human MHC and, in turn, cellular immunity. It establishes a new paradigm for sequencing macaque MHC haplotypes that will likely lead to the solution of many similar haplotypes in the future.

## Results

### MCM M3 haplotype gene content

The complete gene content of the ~5.2-Mb cy0333 genomic region MHC M3 haplotype of MCMs is displayed in Figure 1. This represents the first detailed assembly and annotation focused solely on the MHC genomic region of a macaque in almost two decades since both Daza-Vamenta et al. (2004) and Shiina et al. (2006) characterized the MHC region of a rhesus macaque BAC library (CHORI-250). The cost and labor required to generate and sequence BAC libraries with older sequencing technologies made such studies into this complex and immune-important region prohibitively expensive. The unique limited diversity of the MCM population also enabled the selection of an MHC-homozygous sample, ensuring that the resulting assembly would unambiguously represent a single contiguous macaque MHC haplotype. A total of 383 putative genes

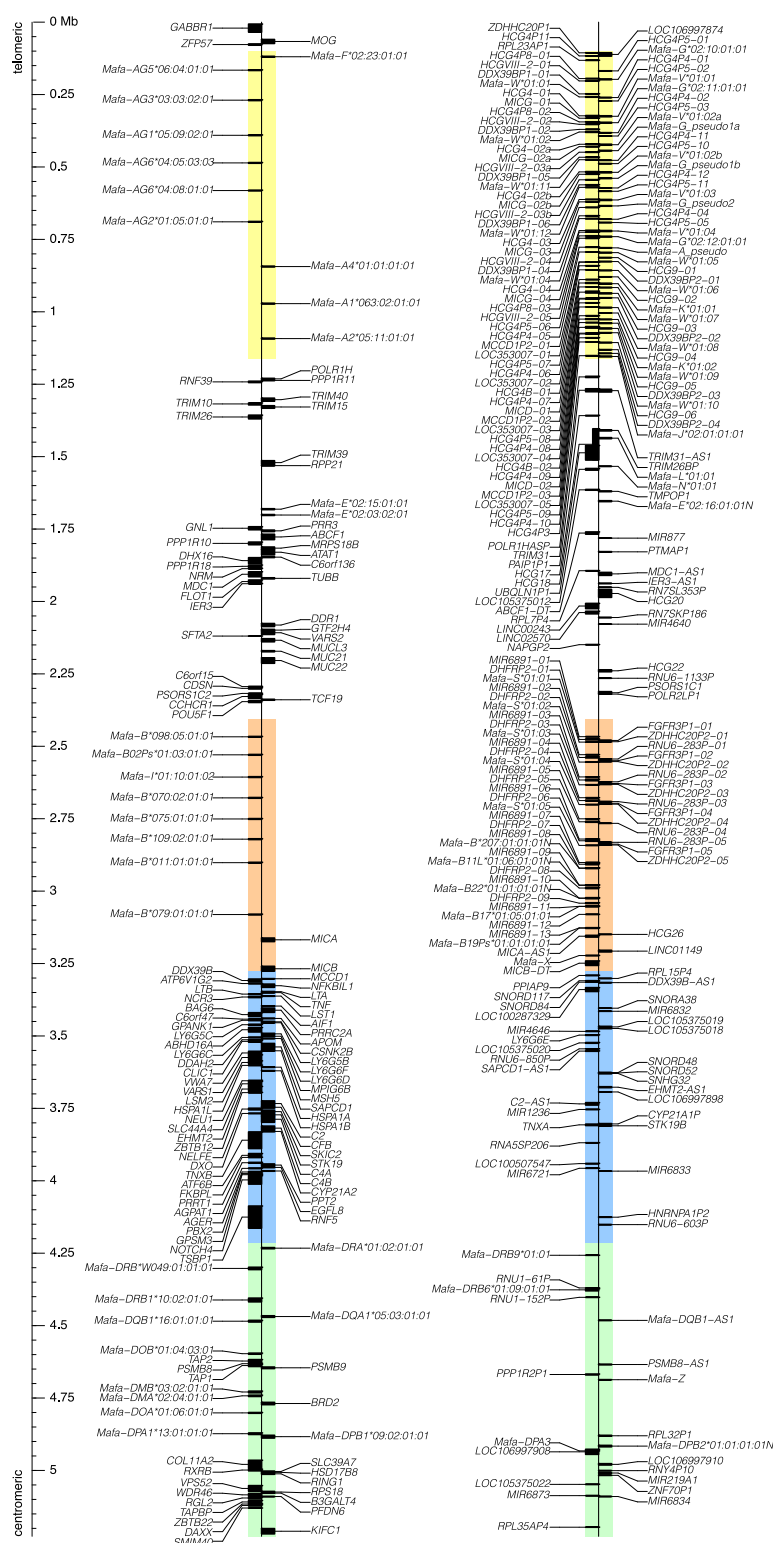


**Figure 1.** Gene content of the cy0333 MHC M3 haplotype of MCM full genomic region. The MHC full genomic region is defined as everything from the telomeric gene *GABBR1* to the centromeric gene *KIFC1*, as per the method of Shiina et al. (2017). Gene content is separated into putatively expressed genes on the left line and noncoding RNAs and pseudogenes on the right line. Gene sequences associated with the telomeric to centromeric sense strand are displayed to the right of each line, and those associated with the antisense strand are displayed to the left. The class I A region is highlighted in yellow; the class I B region is highlighted in orange; the class II region is highlighted in green. The position in megabases is shown on the left.

orthologous to either human or rhesus macaque MHC genes was identified on the cy0333 M3 haplotype (Supplemental Table S1). Of these, 152 contain open reading frames indicative of potential protein expression. This is roughly equivalent to the 305 genes (145 protein-coding) on the human reference genome GRCh38. Although a pair of annotated cynomolgus macaque reference genomes are also currently available (Macaca fascicularis\_5.0; GCF\_000364345 and MFA19.12RKSv2; GCF\_012559485), they were not used to determine gene content of the cy0333 MHC M3 haplotype. The current annotation builds for cynomolgus macaques are not as thorough as human and rhesus macaque MHC region annotations because there are many uncharacterized loci that are difficult to compare to the carefully curated human gene annotations.

Segmental duplications have significantly increased the gene content of the cy0333 M3 haplotype of MCMs within the MHC class I A and class I B regions compared with the human reference genome (Fig. 2). The nomenclature of MHC genes is described in the Supplemental Information. The cy0333 haplotype contains four total *Mafa-A* genes, three of which have canonical classical MHC-I gene open reading frames, and one pseudogene in which the first ~619 nucleotides (nt) of the expected open reading frame (all of exons 1–3) are missing owing to a large deletion event. The *Mafa-B* region experienced even more duplication events than the *Mafa-A* region, with a total of 13 *Mafa-B* genes. Eight of these contain canonical classical MHC class I B gene open reading frames, but the other five cannot be translated into traditional MHC class I B proteins owing to the presence of premature stop codons or frame shifts from the canonical class I B open reading frame.

In addition to differences in classical class I gene content between humans and macaques, there are differences in nonclassical class I genes, namely the *MHC-G* and *MHC-AG* genes. In humans, the *HLA-G* gene is functional; in macaques, all copies of the *MHC-G* gene are pseudogenes with early stop codons introduced in exon 3 (some *MHC-G* genes per macaque haplotype may also lack traditional start sequences; the cy0333 MHC M3 haplotype of MCMs contains three such *Mafa-G* genes). Macaques have instead gained putatively expressed *MHC-AG* genes, which appear

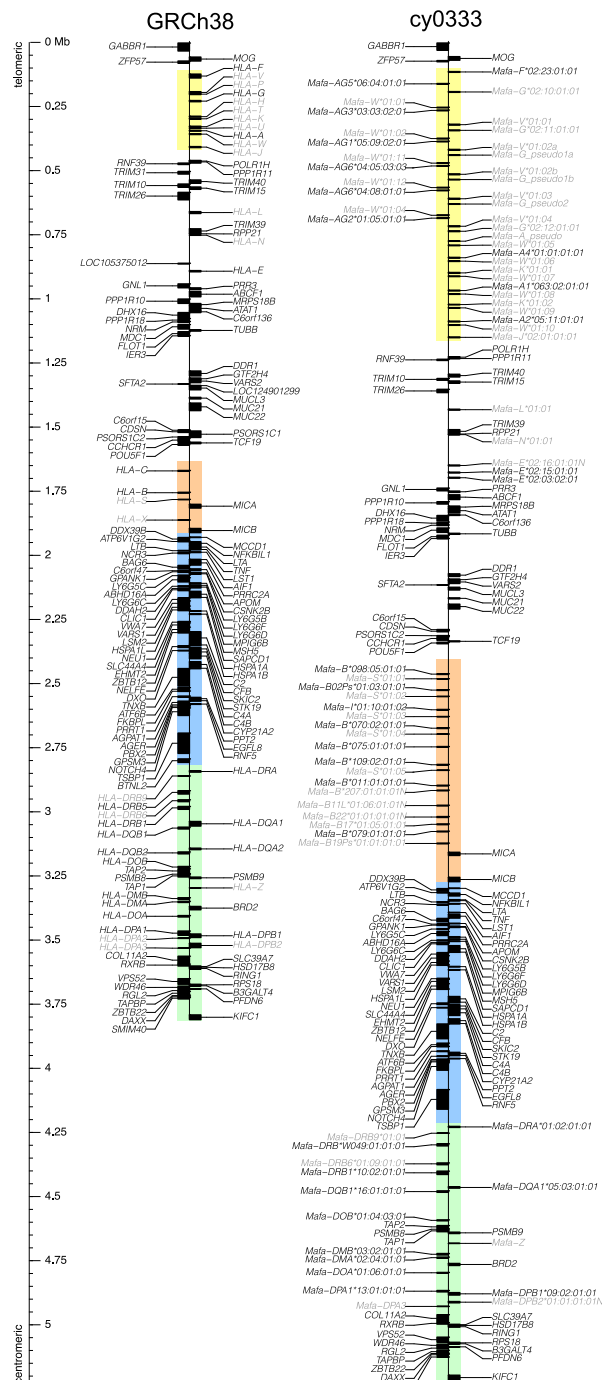


**Figure 2.** Comparison of the representative gene content of the human and the cy0333 MCM full genomic MHC regions. All protein-coding genes plus a subset of nonclassical MHC-I and MHC-II pseudogenes (*MHC-V*, *MHC-W*, *MHC-K*, etc.) and noncoding alleles of otherwise coding genes (*Mafa-B19Ps\*01:01:01:01*, etc.) are shown for the human genome reference GRCh38 (left) and cy0333 (right). Protein-coding genes are shown in black font, and all pseudogenes and nonfunctioning genes are shown in gray font. The class I A region is highlighted in yellow; the class I B region is highlighted in orange; the class III region is highlighted in blue; and the class II region is highlighted in green. Both sequences are equivalently scaled and presented from telomeric genes at the top to centromeric genes at the bottom. Gene sequences associated with the telomeric to centromeric sense strand are displayed to the right of each line, and those associated with the antisense strand are displayed to the left. The relative position in megabases for both sequences is shown on the left.

to be a combination of the 5' end of an *MHC-A* gene (which recovers the stop codon in exon 3) plus the 3' end of an *MHC-G* gene (which maintains the relatively early stop codon in exon 6 that is also observed in the functional *HLA-G* gene). The MHC M3 haplotype of MCMs contains six distinct *Mafa-AG* genes and six duplications of the *Mafa-G* gene. The MCM M3 haplotype also has three total nonclassical class I *Mafa-E* sequences (two expressed *Mafa-E* genes plus one nonexpressed pseudogene *Mafa-E\*02:16:01:01N* lacking a traditional start codon and containing an early stop codon in exon 3). This differing number of segmental duplications is typical for macaques; different haplotypes have undergone different numbers of segmental duplications of classical and nonclassical genes in the class I regions (Daza-Vamenta et al. 2004; Fukami-Kobayashi et al. 2005; Shiina et al. 2006; Otting et al. 2007; Watanabe et al. 2007; Karl et al. 2013; Wiseman et al. 2013; Shortreed et al. 2020).

These segmental duplication events account for most of the ~1.4-Mb length difference between human reference GRCh38 and MCM cy0333; the remaining MHC class III and MHC-II regions are relatively well conserved (Fig. 2). The human HLA region, however, has two regions of significant structural diversity between haplotypes: the complement *C4A/C4B* region and the *HLA-DR* region (Norman et al. 2017). Variable duplications of the *C4* and *HLA-DRB* genes exist on different human haplotypes. The GRCh38 haplotype likely represents one of the shortest forms of HLA class III and class II, with just a pair of *C4* genes (one *C4A* and one *C4B*) as well as a *DR2* haplotype structure (containing *HLA-DRA*, *HLA-DRB9*, *HLA-DRB5*, *HLA-DRB6*, and *HLA-DRB1* genes). An extensive study of HLA haplotype sequence variability noted as many as four *C4* genes within the HLA class III region (Norman et al. 2017). For the *HLA-DR* region, the *DR4* haplotype structure is >300 kb longer than the shortest defined *HLA-DR* haplotypes (Norman et al. 2017). Although the MHC M3 haplotype of MCMs in cy0333 closely resembles the GRCh38 class III and class II structure, with an *MHC-DR* haplotype similar to the *HLA-DR2* haplotype structure (substituting the *Mafa-DRB\*W049:01:01:01* gene into the *HLA-DRB5* gene location), further studies would be necessary to confirm a functional similarity between the MCM M3 *DR* and human *DR2* regions.

All but five of the putatively expressed MHC genes in the human reference genome (*LOC124901299*, *HLA-C*, *BTNL2*, *HLA-DQA2*, and *HLA-DQB2*) appear to have orthologs on the MHC M3 haplotype of MCMs. There are more differences in the content of noncoding RNAs and pseudogenes between the two species, with 56 human noncoding genes appearing to lack a cynomolgus macaque homolog. These pseudogenes may have been lost or gained after humans and macaques diverged.

### Comparison to the MHC region of other macaque reference genomes

We believe that our genomic region assembly of the MHC M3 haplotype of MCMs is the most contiguous macaque MHC region assembly generated to date; there are no gaps or unknown N sequence fillers across the entire 5,227,476 bp. With the advent of high-throughput sequencing more than a decade ago, it became faster and less expensive to sequence whole genomes. This led to many new whole-genome assemblies from Illumina short-read sequence data across multiple model organisms, like one of the representative cynomolgus macaque genomes *Macaca fascicularis*\_5.0 (GCF\_000364345). This genome was assembled from Illumina HiSeq shotgun sequencing reads from a female Indonesian-origin



cynomolgus macaque at ~68× genome coverage in 2013 ([https://www.ncbi.nlm.nih.gov/assembly/GCF\\_000364345.1/](https://www.ncbi.nlm.nih.gov/assembly/GCF_000364345.1/)). Although overall advantageous owing to its relatively low cost and reasonably accurate assembly in nonrepetitive regions, these short reads are insufficient to assemble regions with segmental duplications like the MHC accurately. This is quite apparent when comparing the alignment of our cy0333 MHC M3 haplotype of MCMs to the *Macaca fascicularis*\_5.0 assembly for those regions (Fig. 3). The white bars within the *Macaca fascicularis*\_5.0 reference correspond to gaps of unknown sequence indicated with Ns in the reference sequence. There are 230 total gaps covering at least 373,286 total base pairs out of the 3.9 Mb shown for *Macaca fascicularis*\_5.0, so >9.5% of the reported MHC sequence for this reference genome is unknown.

The full genomic MHC region of *Macaca fascicularis*\_5.0 is also >1.3 Mb shorter than cy0333 and, in particular, lacks gene density within the MHC class I A and class I B regions. There is no reason to believe that the Indonesian cynomolgus macaque sequenced for the *Macaca fascicularis*\_5.0 assembly would not have

a similar MHC-I gene density as the cy0333 M3 haplotype of MCMs. MCMs are most likely derived from a small population of Indonesian cynomolgus macaques, and previous MHC haplotyping studies of cynomolgus macaques from Indonesia, as well as other geographic origins, have shown expected levels of segmental duplications for these regions (Shortreed et al. 2020; de Groot et al. 2022). However, the MHC class I A and class I B regions for *Macaca fascicularis*\_5.0 are both significantly shorter than their cy0333 counterparts.

With the difficulties inherent to the accurate assembly of highly repetitive regions, efforts are underway to improve reference genome assemblies with alternative sequencing technologies like PacBio. These technologies are currently more expensive per base pair than Illumina sequencing but can produce longer reads to assist in the assembly of repetitive regions. The rhesus macaque reference genome released in 2019, Mmul\_10 (GCF\_003339765), was assembled from PacBio RSII sequencing reads from a female Indian rhesus macaque fibroblast cell line at ~66× genome

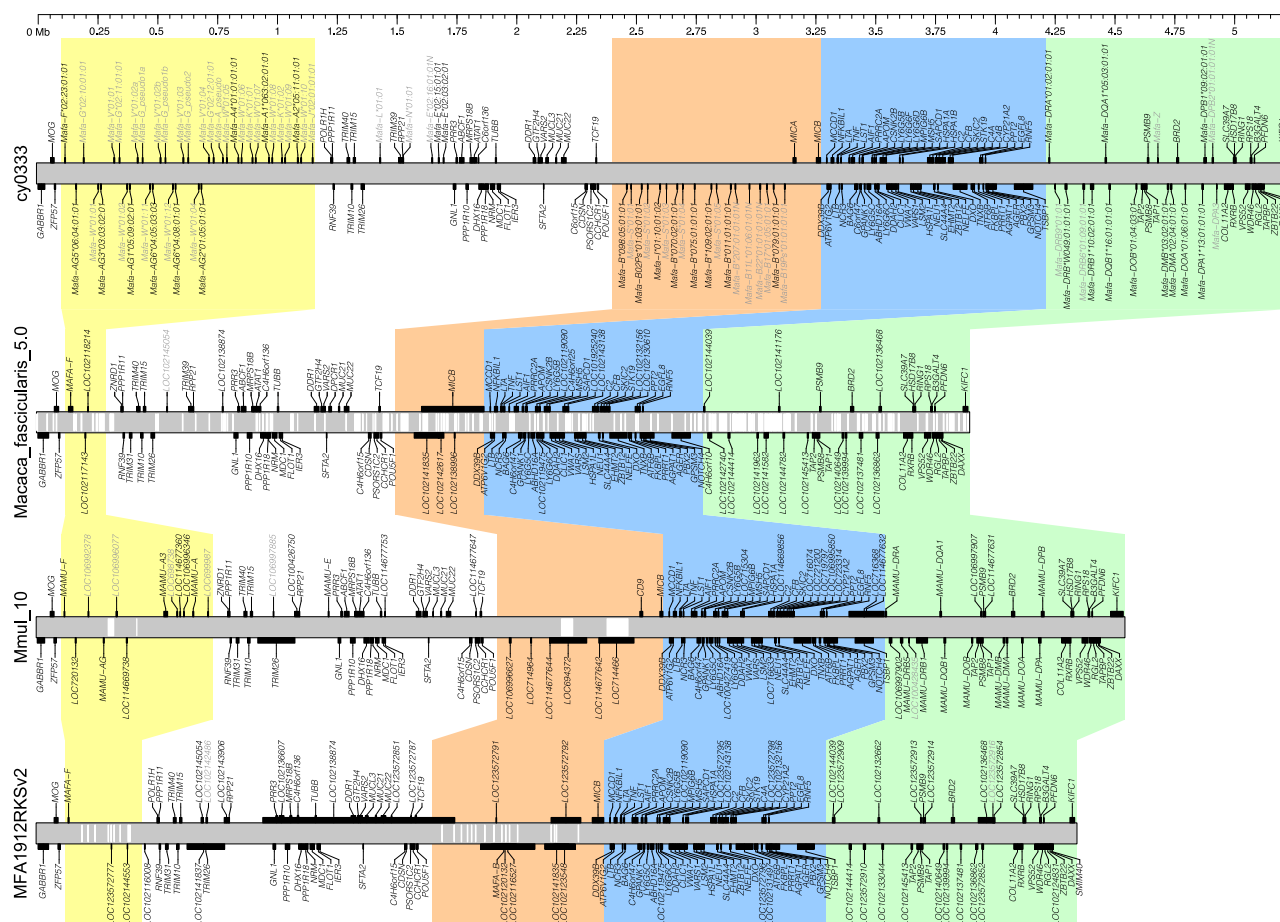


**Figure 3.** Continuity of the cy0333 MCM full genomic MHC region versus three publicly available macaque reference genomes. The cy0333 MHC region (OP204634) is shown in the *top* panel; a cynomolgus macaque reference genome *Macaca fascicularis*\_5.0 (GCF\_000364345) assembled from the Illumina short-read data is shown in the *second* panel down; the rhesus macaque reference genome Mmul\_10 (GCF\_003339765) assembled from the ~13.5-kb PacBio RSII data is shown in the *third* panel down; and a cynomolgus macaque reference genome MFA1912RKSv2 (GCF\_012559485) assembled from the ~12-kb PacBio Sequel II data is shown in the *bottom* panel. Annotations for all protein-coding genes plus a subset of nonclassical MHC-I and MHC-II pseudogenes are shown for each sequence. Protein-coding genes are shown in black font, and pseudogenes are shown in gray font. All sequences are uniformly scaled, and the position in megabases for all sequences is shown across the *top*. Gray tracks represent the sequence for each reference, and white gaps within the gray tracks represent gaps in the assembly. The class I A region is highlighted in yellow; the class I B region is highlighted in orange, the class II region is highlighted in blue; and the class III region is highlighted in green. Gene annotations for *Macaca fascicularis*\_5.0, Mmul\_10, and MFA1912RKSv2 are sourced from and named consistent with NCBI, and gene sizes correspond to the longest predicted translation per gene; some of these predicted translations (particularly the exceptionally long black bars present on some of the references) require further validation and refinement.

coverage (Warren et al. 2020; [https://www.ncbi.nlm.nih.gov/assembly/GCF\\_003339765.1/](https://www.ncbi.nlm.nih.gov/assembly/GCF_003339765.1/)). With average sequence lengths much longer than Illumina at ~13.5 kb, this technology is superior, although still not perfect for the MHC region. Alignment of the MHC region from the Mmul\_10 reference genome to the MCM M3 haplotype shows that it is only ~677 kb shorter than its cy0333 counterpart (Fig. 3). Mmul\_10 contains expanded MHC class I A and class I B regions compared with *Macaca fascicularis*\_5.0, although each region is still shorter than the equivalent region in cy0333. Mmul\_10 also only has four gaps of Ns: two gaps within the class I A region of 22,370 bp and 5 bp, as well as two gaps of 45,930 bp and 86,789 bp within the class I B region (~3.4% of the reported 4.5 Mb of the Mmul\_10 reference MHC full genomic region).

A quality assessment of the Mmul\_10 MHC region showed that the AG07107 fibroblast line used for this assembly was homozygous for the *Mamu-A004* haplotype (the most common MHC class I A haplotype in rhesus macaques) (Warren et al. 2020). The lack of heterozygosity for the genomic region encoding the two functional *Mamu-A* genes of this haplotype made it possible to assemble accurately, harnessing the same advantage we had in assembling the fully homozygous M3 MHC genomic region of cy0333. This localized area of homozygosity resulted in an area of the MHC class I A region that contained no unknown sequence gaps and a relatively clean annotation despite the segmentally duplicated *Mamu-A* genes. The ~22 kb of gaps within the MHC class I A region of Mmul\_10 are near the *Mamu-AG* genes, indicating some uncertainty about the accuracy of the assembly in that portion of the class I A region. The MHC class I B region of Mmul\_10 also includes two relatively large gaps. As presented in the Mmul\_10 primary Chromosome 4 assembly, this region is a fusion of the two MHC class I B haplotypes (*Mamu-B048* and *Mamu-B055*) from the heterozygous AG07107 fibroblasts (Warren et al. 2020). It contains four of the genes expected for the *Mamu-B048* haplotype and two of the genes expected on the *Mamu-B055* haplotype. Most of the remaining *Mamu-B* genes expected for the *Mamu-B048* and *Mamu-B055* haplotypes map to several unlocalized genomic scaffolds associated with the Mmul\_10 whole-genome assembly. Although the MHC-II region is appropriately sized, the gene content again represents a mixture of the two MHC-II haplotypes in the AG07107 fibroblast line, with several of the remaining genes from the alternate haplotype located on additional unlocalized genomic scaffolds.

Another cynomolgus macaque reference genome (MFA1912RKSv2; GCF\_012559485) was assembled from PacBio Sequel II data recently. This assembly was generated from a Cambodian-origin cynomolgus macaque with ~81× genome coverage and sequence read lengths averaging ~12 kb (Jayakumar et al. 2021; [https://www.ncbi.nlm.nih.gov/data-hub/genome/GCF\\_012559485.2/](https://www.ncbi.nlm.nih.gov/data-hub/genome/GCF_012559485.2/)). Comparison to our cy0333 MHC M3 haplotype again highlights a reasonable assembly across areas of less extreme segmental duplications like the MHC class III and MHC-II regions, as well as the MHC-I interval between the class I A and class I B regions (Fig. 3). However, there are once again gaps of Ns within the class I A (nine total gaps) and the class I B (16 total gaps) regions. These gaps are all shown as ~500 bp; lack of variability in gap lengths indicates an extra degree of uncertainty to those gap regions: not only are the precise nucleotides unknown but so are the actual expected gap sizes. Overall, MFA1912RKSv2 contains 12,496 Ns across 4.35 Mb of the MHC full genomic region (~0.3%), but this is likely an underestimate. There are also issues with the current annotations for MFA1912RKSv2, with no annotat-

ed *Mafa-A* genes, only a few *Mafa-B* genes where the predicted translations extend across several of the duplicated *Mafa-B* genes, and an ~800-kb predicted translation for the *Mafa-E* gene *LOC102138874* (along with more appropriately sized predicted translations for that same gene annotation).

Overall, longer reads are easier to assemble accurately, but heterozygosity still complicates de novo assemblies, especially for regions of highly duplicated genes like the MHC class I A and class I B regions. Our hybrid ONT and PacBio HiFi assembly for cy0333 (OP204634) provides a complete and fully annotated alternative genomic reference for the MHC region.

### Classical and nonclassical MHC-I and MHC-II gene content

Previous cDNA studies of MCMs provided a roadmap for expected classical MHC-I and MHC-II gene content for the M3 haplotype (Budde et al. 2010; O'Connor et al. 2010; Wiseman et al. 2013). In those studies, 10 classical class I genes (three *Mafa-A* genes and seven *Mafa-B/I* genes) and seven classical class II genes (two *Mafa-DRB* genes and one gene per locus for *Mafa-DRA*, *Mafa-DQA1*, *Mafa-DQB1*, *Mafa-DPA1*, and *Mafa-DPB1*) were identified. In this study, we detected those 17 expected M3 genes plus seven additional classical class I genes (one *Mafa-A* gene and six *Mafa-B* genes) and five more classical class II genes (two *Mafa-DRB* genes and one gene per locus for *Mafa-DQB1-AS1*, *Mafa-DPA3*, and *Mafa-DPB2*) (Supplemental Table S2). All but two of these additional 12 classical class I and class II genes lack canonical open reading frames and cannot be translated into traditional class I and class II proteins; one of the 12 is a noncoding antisense RNA of the traditional *Mafa-DQB1* locus (*Mafa-DQB1-AS1*). The remaining classical class I gene not previously identified on the MCM M3 haplotype, *Mafa-B02Ps\*01:03:01:01*, does have a canonical seven-exon *Mafa-B* gene open reading frame but appears to be expressed poorly, if at all, in whole blood based on lack of detection in RNA-based genotyping experiments (Budde et al. 2010; Wiseman et al. 2013; Shortreed et al. 2020).

Beyond the classical class I and class II genes, this study also detected the full complement of 19 nonclassical class I and class II genes of the MHC M3 haplotype of MCMs: one *Mafa-F* gene, six *Mafa-AG* genes, five distinct *Mafa-G* pseudogenes, three *Mafa-E* genes (one with a premature stop codon), and one gene each for the *Mafa-DMA*, *Mafa-DMB*, *Mafa-DOA*, and *Mafa-DOB* loci, as well as 27 total distinct MHC-I pseudogenes (one *Mafa-J* pseudogene, two *Mafa-K* pseudogenes, one *Mafa-L* pseudogene, one *Mafa-N* pseudogene, five *Mafa-S* pseudogenes, four *Mafa-V* pseudogenes, 11 *Mafa-W* pseudogenes, one *Mafa-X* pseudogene, and one *Mafa-Z* pseudogene) (Supplemental Table S2).

Three of the class I genes identified on the cy0333 MHC M3 haplotype of MCMs, labeled *Mafa-A\_pseudo*, *Mafa-G\_pseudo1*, and *Mafa-G\_pseudo2*, lack official Immuno Polymorphism Non-Human Primates MHC Database (IPD-MHC NHP) nomenclature because they are peculiar cases. These three pseudogenes are all missing the traditional start codon site owing to large deletions (*Mafa-A\_pseudo* is missing essentially all of exon 1 through intron 3, and both of the *Mafa-G* pseudogenes are missing exon 1 through most of exon 2, only retaining ~37 bp of exon 2), indicating either incomplete duplication of those sequence blocks or large deletion events postduplication. This is in contrast to the other duplicated class I genes lacking traditional open reading frames owing to premature stop codons from internal single-nucleotide polymorphisms or frameshifts within genes with typical start codon

patterns (the other three *Mafa-G* pseudogenes, *Mafa-E\*02:16:01:01N*, and the five *Mafa-B* pseudogenes).

We assessed the nucleotide accuracy of the cy0333 hybrid ONT and PacBio MHC M3 haplotype assembly with independent PacBio sequel II HiFi sequencing of ~2.0- to 4.1-kb gDNA amplicons spanning the full *Mafa-A* or *Mafa-B* genes or exons 2–4 of several of the classical class II genes (*Mafa-DRB*, *Mafa-DQA*, *Mafa-DQB*, *Mafa-DPA*) of cy0333 and three other MCM samples containing the M3 haplotype (Supplemental Fig. S1). These gDNA amplicons cover ~70.8 kb of the cy0333 hybrid ONT and PacBio MHC M3 haplotype assembly and differed at only 2 nt, a single GA dinucleotide repeat within an ~40-bp GA microsatellite sequence located in intron 2 of *Mafa-DRB\*W049:01:01:01*. This equates to an estimated accuracy of 99.997% for the cy0333 hybrid assembly across the ~70.8 kb examined by amplicon sequencing, but as observed directly in our assessment, most of the nucleotide ambiguity occurs in challenging areas like microsatellite repeats and long homopolymers like poly(A) or poly(T) tracks across the full genomic MHC region.

### A potential recent expansion of MHC-I AG/G

The cy0333 MHC M3 haplotype of MCMs shows evidence of a relatively recent segmental duplication event within the class I *Mafa-AG/Mafa-G* region (Fig. 4). There are two distinct instances of a virtually nucleotide-identical ~47-kb block of sequence (differing at only 11 positions across 46,752 nt) containing highly similar *Mafa-V\*01:02* and *Mafa-G\_pseudo1* genes plus three additional pseudogenes. Those blocks are followed by two minimally differentiated ~48.5-kb blocks of sequence located just centromeric to each of the virtually nucleotide-identical *Mafa-G/Mafa-V* blocks. These neighboring blocks contain closely related *Mafa-W* genes (*Mafa-*

*W\*01:11* and *Mafa-W\*01:12*) and *Mafa-AG6* genes (*Mafa-AG6\*04:05:03:03* and *Mafa-AG6\*04:08:01:01*), plus three additional closely related duplicated pseudogenes; these two blocks are ~98.4% identical to each other (in contrast, each of the blocks containing *Mafa-AG6\*04* genes were only ~96.0% and ~90.3% identical to the equivalent flanking blocks containing *Mafa-AG1\*05:09:02:01* and *Mafa-AG2\*01:05:01:01*, respectively). These highly conserved sequence blocks are not just an artifact of incorrect assembly because three independent ONT reads span both of the virtually identical *Mafa-G/Mafa-V* genes (Fig. 4). In fact, one of these ONT reads spans ~546 kb and includes five of the six *Mafa-AG* genes of the M3 haplotype. A comparable recent duplication of the *Mamu-AG* region was previously observed in a well-characterized rhesus macaque MHC BAC library, with only 8-nt substitutions across an ~80-kb sequence block (Daza-Vamenta et al. 2004).

Additional genes within the MHC genomic region have undergone variable degrees of tandem duplication, creating challenges in unambiguously phasing genotypes at the genomic level. For instance, copy number variation in humans has been shown to result in between one and four complement *C4A* (*C4A*) or complement *C4B* (*C4B*) genes per MHC haplotype (Yang et al. 2007). The human *C4* genes lie within genetic units called RCCX modules that each include three flanking genes (*STK19* or *STK19B*, *CYP21A1P* or *CYP21A2*, and *TNXA* or *TNXB*) (Li et al. 2017). The MHC class III region of our assembly contained single *C4A* and *C4B* genes within RCCX blocks (Supplemental Fig. S2). The genomic organization of these duplicated *C4* regions was confirmed by 11 independent ONT reads that completely spanned both *C4* coding regions, and four of these ONT reads spanned both RCCX blocks. Although it is currently unknown whether *C4* copy number variation exists between cynomolgus macaque haplotypes, we are actively assembling additional MHC haplotypes to provide

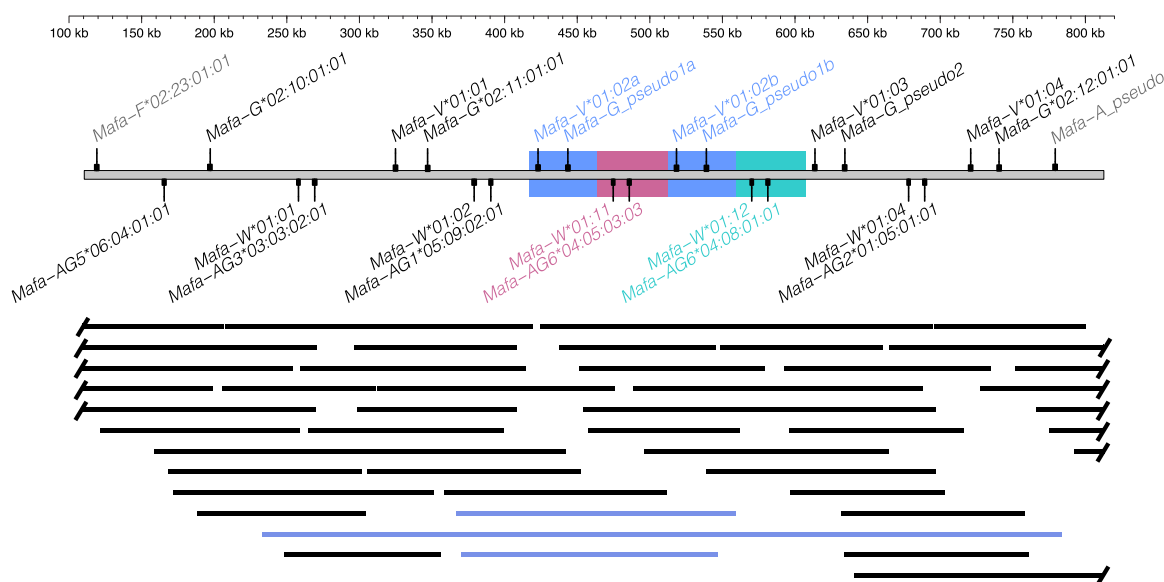


**Figure 4.** Gene content of the cy0333 MHC-I AG/G region. Representative genes and pseudogenes are shown on the gray bar. The blue boxes highlight a virtually nucleotide-identical ~47-kb block of sequence located at two distinct positions within the class I AG/G region; this block contains highly similar *Mafa-V\*01:02* and *Mafa-G\_pseudo1* genes along with three additional pseudogenes not shown. The pink and green boxes highlight closely related (98.4%) ~48.5-kb blocks of sequence located just centromeric to each of the virtually nucleotide-identical *Mafa-G/Mafa-V* blocks. The pink and green boxes contain closely related *Mafa-W* genes (*Mafa-W\*01:11* and *Mafa-W\*01:12*, differing at 20 positions across 2196 nt) and closely related *Mafa-AG6* genes (*Mafa-AG6\*04:05:03:03* and *Mafa-AG6\*04:08:01:01*, differing at 36 positions across 2534 nt), as well as three additional closely related duplicated pseudogenes not shown. The position in kilobases relative to the start of the full genomic MHC region is shown across the top. The bottom portion shows the spans of individual ONT reads located within the class I AG/G region. The three ONT reads shown in blue span both copies of the essentially nucleotide-identical *Mafa-G/Mafa-V* genes.

further insights regarding the genomic organization of the complement gene family in MCMs.

### Specific duplcon structures associated with MHC class I B transcription levels in blood

The MHC class I B region contains 13 total *Mafa-B* genes associated with three different types of duplication blocks varying in the total pseudogene content of the area within and centromeric to each of those *Mafa-B* genes (Fig. 5). It is unknown how these variants in duplication blocks arose: if some of the duplication events were more localized and only included a portion of the surrounding pseudogenes. The first type of duplication block predates the divergence of macaques and humans because it contains the full-pseudogene content consistent with the *HLA-B* gene and its surrounding pseudogenes (*MIR6891*, *DHFRP2*, *RNU6-283P*, *FGFR3P1*, *ZDHHC20P2*, *HLA-S*). The second type of duplication block contains reduced pseudogene content, retaining only two or three of the surrounding pseudogenes, whereas the third type of duplication block only has a variant of the *MIR6891* microRNA located within intron 4 of each *Mafa-B* gene. The two major *Mafa-B* genes detected at high levels in steady-state whole-blood cDNA (*Mafa-B\*075:01:01:01* and *Mafa-B\*011:01:01:01*) are both associated with the second type of duplication block with reduced surrounding pseudogenes (Budde et al. 2010; Wiseman et al. 2013). All five *Mafa-B* genes associated with full-content blocks encode minor transcripts present at low levels when detected in steady-state whole-blood cDNA. The sixth minor *Mafa-B* gene (*Mafa-B\*079:01:01:01*) is the third type of duplication block with just the internal microRNA. The five *Mafa-B* pseudogenes containing atypical open reading frames are all associated with reduced content duplication blocks; two are associated with the second

type of duplication block (with just *MIR6891* and *DHFRP2*), and three are associated with the third type of duplication block (with just the internal microRNA *MIR6891*). Reduced surrounding pseudogene content roughly correlates to higher *Mafa-B* gene expression in steady-state whole blood unless the *Mafa-B* gene contains a premature or late stop codon, rendering it unlikely to be translated into a traditionally functioning MHC-I protein. In comparison, full surrounding pseudogene content (consistent with *HLA-B*) roughly correlates to lower *Mafa-B* gene expression in steady-state whole blood. Those surrounding pseudogenes are located centromeric to the antisense strand *Mafa-B* genes, positioning them upstream of the *Mafa-B* start codon.

A review of the *MHC-B* region in three other great ape reference genomes shows that equivalents to the full-content human *HLA-B* duplication block are also present in the western gorilla reference genome (*Gorilla gorilla*; GCF\_008122165) and for one of the three *MHC-B* genes annotated in the Sumatran orangutan reference genome (*Pongo abelii*; GCF\_002880775) (Supplemental Fig. S3). The other two Sumatran orangutan *MHC-B* genes plus the *MHC-B* gene cluster observed in the chimpanzee reference genome (*Pan troglodytes*; GCF\_002880755) also display essentially this full duplication block, minus only the *MHC-S* gene located on the centromeric-most end of the gene cluster. This full-content *MHC-B* gene block therefore represents the probable *MHC-B* gene content of the most recent common ancestor between macaques and great apes. Duplication blocks with full- or near-full-pseudogene content likely represent the oldest *MHC-B* genes on each haplotype, with pseudogenes lost from duplication blocks in subsequent more recent segmental duplication events.

None of the 13 *Mafa-B* gene duplication blocks contain pseudogene content consistent with the *HLA-C* gene and its surrounding pseudogenes (*USP8P1*, *RPL3P2*, *WASF5P*, *LINC02571*, and

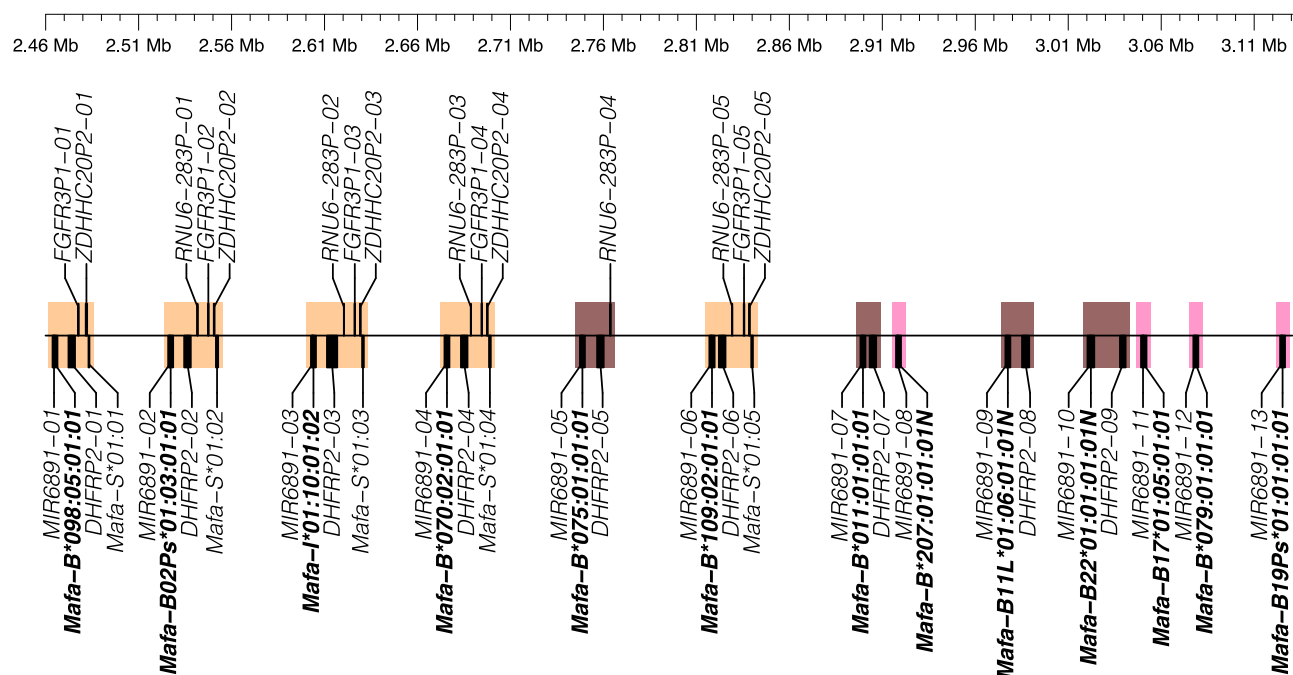


**Figure 5.** Gene content of the cy0333 MHC class I B region. Blocks of duplicated genes and pseudogenes are shaded. Orange shading indicates blocks containing essentially all six pseudogenes surrounding the classical class I *Mafa-B* gene, consistent with the pseudogenes surrounding the human *HLA-B* gene. Brown shading indicates blocks containing only two or three of the surrounding pseudogenes plus the *Mafa-B* gene. Pink shading indicates blocks containing only the *Mafa-B* gene and a microRNA located within intron 4 of the *Mafa-B* gene. *Mafa-B* allele names are displayed in bold. Position in megabases relative to the start of the full genomic MHC region is shown across the top.



*LOC112267902* (Supplemental Table S1). This is not unexpected because *HLA-C* homologs have only been identified in great apes. It is thought that *HLA-C* and *HLA-B* developed from a common ancestral gene after apes and Old World monkeys like macaques diverged (Adams and Parham 2001; Fukami-Kobayashi et al. 2005).

## Discussion

### Utility of a highly accurate macaque MHC full genomic region assembly

The unambiguously assembled, contiguous, and highly accurate cy0333 MHC M3 haplotype of MCMs presented here provides a valuable genomic region reference sequence. Although the human HLA full genomic region serves reasonably well much of the time as a reference for extracting sequencing reads from a macaque data set for downstream de novo assembly, macaques may contain blocks of sequence within their MHC region that differ substantially enough from the human HLA region, where no reads spanning that region will be extracted. We observed this directly when extracting the reads for error correction of our cy0333 MHC M3 region haplotype; a second round of mapping PacBio reads to our cy0333 assembly was required to extract additional reads to fill in a few areas left uncovered with the initial HLA mapping. Using the cy0333 MHC haplotype as the reference for future extractions of macaque sequence reads should substantially reduce this issue. The cy0333 MHC full genomic region haplotype is also suitable as a reference for mapping whole-exome short reads from other macaque samples and is a helpful resource for designing amplicon primers, probes for target capture, or CRISPR-Cas9-targeted enrichment as has recently been reported for macaque killer-cell immunoglobulin-like receptors (KIR) gene clusters (Bruijnesteijn et al. 2021). The assembly of the full MHC genomic region from a homozygous macaque provides unequivocal confirmation that this cy0333 haplotype reference is an accurate ~5.2-Mb end-to-end layout of the MHC M3 haplotype of MCMs with no genes from other haplotypes mixed in, no genes expected on the M3 haplotype mapped to any secondary scaffolds, and no question of the validity of the assembly even with identical or highly similar sequence present more than once across the haplotype. This is especially valuable for assessing the gene content of the heavily duplicated MHC class I A and class I B regions. Additionally, the high accuracy of the PacBio HiFi reads generated for this assembly is valuable for distinguishing functional from nonfunctional genes, where single-nucleotide accuracy is vital for confirming true polymorphisms that introduce early stop codons into otherwise presumably functional genes.

### Classical MHC-I gene insights

When considering the wealth of class I genes carried on each MHC haplotype in macaques, we find it helpful to divide them into major versus minor allele lineages based on their steady-state RNA levels in whole blood. For the MHC M3 haplotype of MCMs, these major alleles include *Mafa-A1\*063:02:01:01*, *Mafa-B\*075:01:01:01*, and *Mafa-B\*011:01:01:01*. They appear to function like the *HLA-A* and *HLA-B* genes in humans and are responsible for the bulk of antigen presentation to CD8<sup>+</sup> T cells (Loffredo et al. 2009; Budde et al. 2011). The number of major alleles varies between macaque MHC-I haplotypes; a single major A1 allele and two to four major B alleles per haplotype are commonly observed (Shortreed et al. 2020). The minor alleles of the M3 haplotype include *Mafa-*

*A2\*05:11:01:01*, *Mafa-A4\*01:01:01:01*, *Mafa-B\*070:02:01:01*, *Mafa-B\*079:01:01:01*, *Mafa-B\*098:05:01:01*, *Mafa-B\*109:02:01:01*, and *Mafa-I\*01:10:01:02*. Steady-state RNA levels for these minor alleles are reduced from fivefold to more than 100-fold relative to the major alleles (Budde et al. 2011). Although they are present in variable numbers and combinations on every macaque MHC-I haplotype, the roles of these minor alleles in cellular immune responses remain elusive. In contrast to major allele lineages, the minor allele lineages tend to be distinguished by numerous allelic variants that are distributed across a wide variety of haplotypes (Supplemental Table S2). For example, the July 2022 IPD-MHC NHP database (release 3.9.0.1 [2022-07] build 209) includes 95 and 85 distinct allelic variants of the *Mafa-A2\*05* and *Mamu-A2\*05* lineages, respectively. Likewise, characterization of a large breeding colony of Indonesian cynomolgus macaques revealed that nearly two-thirds (45/70) of the high-resolution *Mafa-A* haplotypes segregating in this population included one of at least 25 distinct *Mafa-A2\*05* allelic variants (Shortreed et al. 2020). At least one member of the *A2\*05* lineage (*Mamu-A2\*05:01*) has been shown to have the capacity to present simian immunodeficiency virus (SIV) epitopes (de Groot et al. 2017). Further studies will be required to untangle the full functions of these prevalent minor alleles such as *A2\*05* in macaques.

Another long-standing puzzle that remains regarding the expansion of the MHC-I region described here is how macaques balance the maintenance of a sufficient repertoire of T cell receptors to respond to a diversity of pathogens with negative selection to remove potentially autoreactive T cells (Daza-Vamenta et al. 2004). The collection of *Mafa-B* pseudogenes on the M3 haplotype provides a glimpse into this evolutionary balancing act. The loss of protein-coding potential for these class I pseudogenes has occurred owing to an array of mechanisms. The first of these is exemplified with the *Mafa-B\*207:01:01:01N* and *Mafa-B19Ps\*01:01:01:01* alleles that have lost the appropriate in-frame ATG start codon owing to single-nucleotide variants. This appears to be an ongoing process of inactivation for the *Mafa-B\*207* lineage because the internal in-frame start codon has also been disrupted for a second member of this lineage (*Mafa-B\*207:03:01:01*), but it is still intact for the closely related *Mafa-B\*207:02:01:01* allele that retains the ability to encode a canonical class I protein. The IPD-MHC NHP database currently lacks other members of the *Mafa-B19Ps* lineage besides the *Mafa-B19Ps\*01:01:01:01* pseudogene. However, there is a *Mamu* homolog (accession AB128842) of this *Mafa-B19Ps* pseudogene that was characterized as part of the complete rhesus macaque haplotype from the CHORI-250 BAC library (Daza-Vamenta et al. 2004; Shiina et al. 2006). Because both of these *B19Ps* pseudogenes carry identical start codon disruptions, this variant is likely to pre-date the speciation of cynomolgus and rhesus macaques >2 Myr ago. A second common mechanism of pseudogene formation is the introduction of a premature stop codon owing to a single-nucleotide variant in the coding region. The *Mafa-B22\*01:01:01:01N* and *Mafa-B11L\*01:06:01:01N* alleles of the M3 haplotype exemplify this mechanism with premature stop codons in exons 2 and 4, respectively. Another deviation from the traditional *MHC-B* open reading frame is observed in *Mafa-B17\*01:05:01:01*. There is a single-nucleotide deletion in the first codon of exon 6 of this allele, causing a frameshift through the rest of the open reading frame and loss of the typical *MHC-B* stop codon within exon 7. Because splicing sites compatible with the typical *MHC-B* exon 8 are retained, *Mafa-B17\*01:05:01:01* would reach a stop codon 129 bp into the normal 3' untranslated region and have a much longer cytoplasmic tail that is completely distinct

from classical class I B proteins. Transcriptional silencing could reflect yet another mechanism that may have led to the loss of functional class I protein production for the *Mafa-B02Ps\*01:03:01:01* gene on the M3 haplotype. The IPD-MHC NHP database currently includes 17 *Mafa* and 24 *Mamu* full-length genomic alleles for this *B02Ps* lineage whose first representative alleles were deposited in 2010. Although cDNA sequences for this putative pseudogene lineage have yet to be detected despite exhaustive efforts by our group and other investigators, the mechanism of this transcriptional silencing phenomenon remains to be defined. It is also possible that *Mafa-B02Ps\*01:03:01:01* only uses robust tissue-specific expression, or expression in a distinct leukocyte subset, and thus was not detected in studies of RNA isolated from cells present in whole blood (Greene et al. 2011).

### Nonclassical MHC-I gene insights

Nonclassical MHC-I genes are often studied in the context of natural killer (NK) cell engagement. We characterized six distinct *Mafa-AG* alleles at the telomeric end of the MHC class I A region of cy0333. This region was organized into ~40- to 80-kb genomic blocks with close sequence identity, suggesting recent segmental duplication of the *Mafa-AG* locus. The *Mafa-AG* gene is believed to have functionally replaced the role of *HLA-G* in humans. Both genes are primarily expressed on the surface of invasive extravillous trophoblasts of the placenta and are thought to regulate the maternal immune response to pregnancy through the engagement of NK receptors. Indeed, rhesus macaque *Mamu-AG2\*01:01* has been shown to have broad recognition by KIR genes *KIR3DL05*, *KIR3DL07*, *KIR3DS01*, *KIR3DS02*, *KIR3DSw07*, and *KIR3DSw09* (Nicholas et al. 2022; Anderson et al. 2022). Given the expansion of lineage II KIRs in macaques, it is not surprising that the *MHC-AG* gene has also undergone tandem duplication events relative to the single-copy *HLA-G* gene (de Groot et al. 2015). Our findings further implicate the close evolutionary relationship between the NK cell receptor and nonclassical *MHC-AG* gene clusters.

We also characterized three nonclassical class I *Mafa-E* sequences associated with the MHC M3 haplotype of MCMs: two with complete traditional open reading frames and one noncoding pseudogene. The ability of MHC-E proteins to present MHC-I signal-sequence and pathogen-derived peptides to NK and CD8<sup>+</sup> T cells is conserved between primate species (Wu et al. 2018). Cell surface expression of *MHC-E* can be induced by cytomegalovirus (CMV), and *MHC-E* has become a crucial target for CMV-based vaccine development (Tomasec et al. 2000; Voogd et al. 2022). Studies have shown that 55% of rhesus macaques were completely protected against SIV challenge after vaccination with CMV/SIV vectors and that the protection was mediated by *MHC-E*-restricted antigen recognition by CD8<sup>+</sup> T cells (Hansen et al. 2011, 2013; Malouli et al. 2021). Genetic variation within *Mamu-E* genes has been shown to be significantly associated with a lack of CMV/SIV vaccine protection in this model (Brochu et al. 2022). *MHC-E* also presents peptides to NKG2/CD94 heterodimers on the surface of NK cells. CD94/NKG2C<sup>+</sup> NK clonal populations proliferate in response to CMV infection, suggesting an adaptive-like NK cell immune response with antigen specificity (Gumá et al. 2004; Rölle et al. 2014). Furthermore, these expanded NK cell populations can form long-lived memory cells that provide increased protection following subsequent CMV challenge (Sun et al. 2009). Given this association, the simplified genetics of MCMs may serve as a better model system to dissect the genetic basis of protection in

CMV-based vaccination studies. Furthermore, the examination of transposable elements, untranslated region sequences, and intronic polymorphisms from multiple MHC genomic haplotypes within the MCM population may provide a clearer image of the genetic determinants of vaccine-mediated protection.

### Caveats and future directions

Since the conception of this paper, a new ONT base caller, Remora, with marginally higher single-nucleotide accuracy was commercially released (<https://github.com/nanoporetech/remora>). Although higher accuracy base calls will theoretically benefit the ONT assembly process, we are confident that our hybrid assembly does not require the marginal gains of Remora owing to the end-to-end PacBio HiFi coverage used in error correction. We assessed the accuracy of MHC-I and MHC-II genes in our hybrid cy0333 assembly versus gDNA amplicon sequences and found 99.997% concordance, with the only variance occurring within a short tandem repeat. Although single-nucleotide accuracy is improved with Remora, it remains to be seen if similar accuracy gains are achieved in difficult areas like repetitive motifs.

Alternate assembly algorithms such as Flye and WENGAN-D can produce highly accurate assemblies using multiple sequencing technologies (Kolmogorov et al. 2019; Di Genova et al. 2021). We used both Flye and WENGAN-D in our initial assembly attempts and found both incapable of assembling the highly duplicated *MHC-AG* region. In contrast, Canu was capable of properly untangling the *MHC-AG* region, which we confirmed by manually inspecting ONT reads spanning the neighboring, near-identical *Mafa-AG* genomic blocks (Koren et al. 2017; Nurk et al. 2020). Therefore, for our purposes, Canu seems to be the most capable of handling highly repetitive genomic regions.

The approach to de novo MHC full genomic region assembly through whole-genome sequencing is admittedly cost-prohibitive for large-scale MHC haplotype characterization of large cohorts of animals. Recently, Cas9 enrichment was used to create haplotype-phased genomic assemblies of rhesus macaque KIR regions (Bruijnesteijn et al. 2021). A similar approach can most likely be applied to MHC enrichment; however, we forwent region-specific enrichment in favor of unbiased, whole-genome sequencing in order to create assemblies of multiple regions from the same animal. Sequencing all of the immune-important gene clusters (spread across different chromosomes) from the same animal might point to insights into specific protein interactions that would be lost when examining each genomic region independently from different samples.

The method presented here for assembling the cy0333 MHC M3 haplotype of MCMs from ultralong ONT and highly accurate PacBio HiFi sequencing reads is being directly applied to resolving the full MHC genomic regions of the remaining six haplotypes in the MCM population, including the most abundant M1 haplotype (accounting for 19.8% of overall MHC haplotypes in MCMs) (Wiseman et al. 2013). It can also be extended to the characterization of sire–dam–offspring trios from additional nonhuman primate species in which sequence reads can be binned to assemble appropriately phased haplotypes per animal to avoid chimeric MHC assemblies. With additional unambiguous full-macaque MHC regions solved, it may be possible to assess any potential genomic cues for major versus minor differential expression of the MHC-I genes in steady-state RNA from whole blood. Finally, this method can also potentially be extended to assembly and annotation of other immune-important genomic regions of macaques

such as the leukocyte receptor complex and KIRs, NK complex, Fc gamma receptors, T cell receptors, and immunoglobulin gene clusters. Together with the restricted genetic diversity of the MCM population, the development of these new genomic resources will provide exceptional opportunities to improve the design and reproducibility of a wide variety of biomedical research.

## Methods

### Samples

Splenocytes and peripheral blood mononuclear cells (PBMC) were obtained from a MCM (cy0333) housed at the Wisconsin National Primate Research Center. This macaque was previously genotyped as M3 homozygous in the MHC region (Ericson et al. 2014). Analysis of SNP patterns in the whole-genome sequence data for cy0333 showed that the homozygous region of Chromosome 4 containing the MHC extends over an interval of ~11 Mb (see Supplemental Information; Supplemental Table S3). Sampling was performed following protocols approved by the University of Wisconsin–Madison Institutional Animal Care and Use Committee and in accordance with the regulations and guidelines outlined in the Animal Welfare Act, the Guide for the Care and Use of Laboratory Animals, and the Weatherall report (Weatherall 2006).

### High-molecular-weight DNA extraction for Oxford Nanopore sequencing

DNA was extracted from frozen splenocytes or PBMC using slight modifications of a previously described ultralong DNA extraction protocol (Jain et al. 2018). Per extraction,  $2 \times 10^7$  cells were thawed and spun at 300g for 10 min. Pelleted cells were resuspended in 200  $\mu$ L PBS by pipette mixing. Resuspended cells plus 10 mL TLB (100 mM NaCl, 10 mM Tris-Cl at pH 8.0, 25 mM EDTA at pH 8.0, 0.5% (w/v) SDS, 20  $\mu$ g/mL Qiagen RNase A, H<sub>2</sub>O) were combined in a 15-mL conical tube and vortexed at full speed for 5 sec. Samples were incubated for 1 h at 37°C. Qiagen Proteinase K (200  $\mu$ g/mL) was added and mixed by slow end-over-end inversion three times. Samples were incubated for 2 h at 50°C with 3 $\times$  end-over-end inversion every 30 min. The lysate was slowly pipetted into two phase-lock 15-mL conical tubes (prepared by adding ~2 mL autoclaved high-vacuum silicone grease into 15-mL conical tubes and spinning max speed for 1 min to move the grease to the bottom of the tube), adding a 5 mL sample to each tube. To each phase-lock tube of lysate, 2.5 mL buffer-saturated phenol and 2.5 mL chloroform were added before rotational mixing at 20 rpm for 10 min. Tubes were then spun down at 4000 rpm for 10 min in an Eppendorf 5810R centrifuge with a swing-bucket rotor. After centrifugation, the aqueous phase above the silicone grease from each conical tube was poured into a new phase-lock 15-mL conical tube. The addition of phenol and chloroform, rotational mixing, and centrifugation were repeated with the second set of phase-lock tubes. The aqueous phases from both phase-lock tubes were slowly poured into a single 50-mL conical tube before adding 4 mL of ammonium acetate (5 M) and 30 mL of ice-cold 100% ethanol. The mixture was incubated at room temperature, whereas the DNA visibly precipitated. Once the DNA rose to the surface of the mixture, a glass capillary hook was used to retrieve the DNA. The hooked DNA was dipped into 70% ethanol to tighten the DNA into an opaque pellet on the hook and then carefully worked off of the hook into an Eppendorf DNA LoBind 1.5-mL tube. To wash the DNA pellet, 1 mL of 70% ethanol was added to the tube before spinning down at 10,000g for 1 min and then removing as much ethanol as possible. This process was repeated for a second 70% ethanol wash,

and any remaining ethanol was evaporated off during a 15-min incubation at room temperature. Finally, 100  $\mu$ L of elution buffer (10 mM Tris-Cl at pH 8.0, H<sub>2</sub>O) was added before incubating the DNA at 4°C for at least 2 d to resuspend fully. A total of 11 ultralong DNA isolations were performed to obtain enough product for ONT sequencing.

### High-molecular-weight DNA extraction for PacBio HiFi sequencing

DNA was extracted from PBMC using New England Biolabs' Monarch high-molecular-weight DNA extraction kit for cells and blood following the manufacturer's protocol. Briefly,  $5 \times 10^6$  PBMCs were pelleted by centrifugation for 3 min at 1000g. One hundred fifty microliters of nuclei prep solution was added to the resuspended pellet and pipetted 10 times up and down to mix; 150  $\mu$ L of nuclei lysis solution was added and inverted 10 times to mix. Each sample was incubated for 10 min at 56°C in a thermal mixer at 2000 rpm. Following incubation, 75  $\mu$ L of precipitation buffer was added, and the solution was inverted 10 $\times$  to mix. Two DNA capture beads were added to each sample, followed by 275  $\mu$ L of isopropanol. Samples were inverted on a vertical rotating mixer at 10 rpm for 8 min. The liquid was pipetted from the samples, avoiding gDNA wrapped around the capture beads. Two washing steps were performed by adding 500  $\mu$ L of DNA wash buffer, inverting three times, then carefully removing the wash buffer by pipetting while avoiding the DNA capture beads. Following washes, the beads were poured into a supplied bead retainer and pulse spun for ~1 sec. The separated glass beads, along with 100  $\mu$ L of elution buffer, were added to a 2-mL microfuge tube and incubated for 5 min at 56°C in a thermal mixer at 300 rpm. After incubation, the eluate was separated from DNA capture beads using the supplied bead retainer and poured into an Eppendorf DNA LoBind 1.5-mL tube. The bead retainer and 1.5-mL tube were centrifuged for 1 min at 12,000g to separate eluate from DNA capture beads. The final eluate with DNA was stored at 4°C until library preparation.

### Library preparation for ONT

Ultralong DNA was prepared for sequencing on ONT R9.4 MinION flow cells using the SQK-RAD004 rapid sequencing kit with modifications of a previously described library preparation optimized for the RAD004 sequencing kit (Jain et al. 2018). A 16  $\mu$ L aliquot of DNA was pipetted as slowly as possible, using a cut-off P20 pipette tip, into a 0.2-mL PCR tube. One microliter of that DNA aliquot was used for quantification using the Thermo Fisher Scientific Qubit dsDNA BR assay kit. Because of the heterogeneity of ultralong DNA, concentrations for the same DNA isolation were highly variable. Qubit concentrations ranged from 43.6 ng/ $\mu$ L to 450 ng/ $\mu$ L per quantified aliquot, with an average concentration of 231.1 ng/ $\mu$ L across all aliquots. To the remaining 15  $\mu$ L of DNA in the PCR tube, 1.5  $\mu$ L fragmentation mix (FRA) and 3.5  $\mu$ L elution buffer were added and then pipetted up and down as slowly as possible 8 $\times$  to mix using the cut-off P20 pipette tip. The sample mixture was thermal cycled for 1 min at 30°C, for 1 min at 80°C, and then a 4°C hold to perform the fragmentation. One microliter of rapid adapter (RAP) was added and then pipetted up and down as slowly as possible 8 $\times$  using the cut-off P20 pipette tip to mix. The DNA mixture was incubated at room temperature while the flow cell was primed. Flow cell priming was performed by adding 30  $\mu$ L of flush tether (FLT) to a tube of flush buffer (FB) and then vortexing the FB tube and briefly spinning it down. A flow cell check was performed; then a tiny volume of storage buffer was removed from the flow cell, and 800  $\mu$ L of flush mix

was added through the priming port following the manufacturer's instructions. After 5 min, the SpotON port was opened, and another 200  $\mu$ L of flush mix was added through the priming port, watching for a small amount of liquid to bead up through the SpotON port. Returning to the DNA mixture, 34  $\mu$ L sequencing buffer (SQB) and 20  $\mu$ L H<sub>2</sub>O were added and slowly pipetted up and down five times with a wide-bore P200 pipette tip to mix. The final DNA mixture was then loaded dropwise into the SpotON port for diffusion loading of the MinION flow cell.

### MinION sequencing and base calling

Sixty R9.4 (FLO-MIN106) MinION flow cells of ultralong DNA were sequenced according to ONT guidelines using their MinKNOW software to control each sequencing run. Different versions of MinKNOW were used throughout the course of the study as updates were released; specific versions are recorded in the meta-data in the FAST5 files for each run. Base calling was performed using Bonito version 0.3.8 on A100 GPU hardware running CUDA 11.2.

### PacBio Sequel II sequencing

High-molecular-weight DNA was provided to the University of Wisconsin–Madison Biotechnology Center DNA Sequencing Facility. The quality of the extracted DNA was measured on a Thermo Fisher Scientific NanoDrop One instrument. Concentrations, 260/230 ratios, and 260/280 ratios were logged. Quantification of the extracted DNA was measured using the Thermo Fisher Scientific Qubit dsDNA high-sensitivity kit. Samples were diluted before running on the Agilent FemtoPulse system to assess DNA sizing and quality. A PacBio HiFi library was prepared according to PN 101-853-100 version 03 (PacBio). Modifications include shearing with Covaris gTUBEs and size selection with Sage Sciences BluePippin. Library quality was assessed using the Agilent FemtoPulse system. The library was quantified using the Qubit dsDNA high-sensitivity kit. The library was sequenced on a PacBio Sequel II instrument using the sequel polymerase binding kit 2.2 at the University of Wisconsin–Madison Biotechnology Center DNA Sequencing Facility. Raw sequencing data were converted to circular consensus sequencing (CCS) FASTQ using SMRT Link version 8.0.

### Hybrid de novo assembly of the MHC region

ONT and PacBio HiFi FASTQ reads were mapped against the human reference genome GRCh38 (GCA\_000001405) using minimap2 version 2.17 (Li 2018) using the “-ax map-ont” and “-ax map-hifi” flags, respectively. Reads mapping to coordinates Chr 6: 29,400,000–33,525,000 (the coordinates for the genes bounding the full genomic HLA region, *GABBR1* through *KIFC1* [Shiina et al. 2017], plus ~200 kb of sequence on both ends) were extracted using SAMtools version 1.11 (Li et al. 2009) and converted back to FASTQ using BBTools reformat.sh (<https://sourceforge.net/projects/bbmap/>). Extracted ONT and PacBio reads were assembled separately using Flye version 2.7 using the “--genome-size 5m” and “--nano-corr” or “--pacbio-hifi” flags. After assembling, the ONT-only and PacBio-only contigs were merged using quickmerge version 0.3 (<https://github.com/mahulchak/quickmerge>) to produce a hybrid assembly. This assembly produced seven total contigs, the longest being ~5.4 Mb. Upon closer investigation of the longest hybrid contig, we noticed a break within the *Mafa-AG* region. Based on our previous experience with the MHC regions of macaques, we were aware that the *Mafa-AG* duplicons within the MHC class I A region are challenging to resolve owing to the potential for large blocks of highly similar sequence (Boyson et al. 1999; Daza-Vamenta et al. 2004; Shiina et al. 2006). We therefore decid-

ed that Flye by itself may not be capable of properly assembling this highly repetitive genomic region and that Canu may serve as a better alternative for this region. To attempt to better focus a second de novo assembly on the region where the previous assembly broke, reads mapping to coordinates Chr 6: 29,400,000–30,033,000 (the coordinates for the genes bounding the HLA class I A region, *GABBR1* through *POLRIH* [Shiina et al. 2017], plus flanking sequence) were extracted and assembled separately using Canu version 2.2 with the “-genomeSize=1m” and “-nanopore” or “-pacbio-hifi” flags, respectively. ONT and PacBio contigs were then merged using quickmerge version 0.3. The second assembly produced a single ~1.5-Mb contig. A comparison between the initial full genomic MHC region assembly and the secondary class I A-focused assembly showed excellent concordance in the areas of overlap; the two assemblies were then manually combined at the start of the predicted *Mafa-I* gene to create one scaffold 5,227,476 bp in total length, spanning from *GABBR1* through *KIFC1*. Metrics for numbers of ONT and PacBio reads at or above various lengths for both the MHC region and the whole genome are shown in Supplemental Table S4, and read coverage for ONT and PacBio across the full genomic MHC region are shown in Supplemental Figure S4.

### PacBio HiFi polishing

First-round error correction was performed using the extracted PacBio HiFi reads that aligned to human coordinates Chr 6: 29,400,000–33,525,000 with Geneious Prime v 2022.1.1 (<https://www.geneious.com/>). The Geneious mapper was used with custom sensitivity and iteration up to 10 times for fine-tuning. Several advanced custom settings were enabled: Map multiple best matches to none; trim paired read overhangs; only map paired reads that both map; allow a maximum of 10% gaps per read with maximum gap size of 15, word length of 18, and index word length of 13; ignore words repeated more than 12 times; maximum of 5% mismatches per read; maximum ambiguity of four; and accurately map reads with errors to repeat regions. A consensus sequence for that mapping was generated in Geneious Prime using a 0% (majority) threshold, assigning total quality and calling the reference (the hybrid scaffold) if no coverage and calling the reference if coverage was less than five reads. The resulting consensus sequence was thus corrected to correspond to higher-accuracy PacBio HiFi reads at any positions where the PacBio data differed from the hybrid assembly, provided the PacBio coverage was greater than five reads. A few areas of the hybrid assembly lacked any PacBio coverage and thus remained uncorrected. These regions presumably corresponded to areas of the macaque MHC that differed substantially from the human HLA region. To address these areas, we performed a second round of PacBio mapping using minimap2 and extracted reads that aligned to the first-round error corrected hybrid assembly. This new set of PacBio reads was then used to error correct a second time and fill in gaps left by the HLA-extracted PacBio reads. The final mapping resulted in end-to-end, >5× PacBio coverage across the entire ~5.2-Mb hybrid assembly (Supplemental Fig. S4).

### Gene annotation

We used the sequence comparison tool Exonerate version 2.4.0 using the “est2genome” mapping model (<https://www.ebi.ac.uk/about/vertebrate-genomics/software/exonerate>). Exonerate was run recursively using three different sequence lists: human gene and CDS annotations from GRCh38.p12, rhesus macaque MHC-I region CDS annotations from CHORI-250 BAC library from the NCBI GenBank (<https://www.ncbi.nlm.nih.gov/genbank/>)



sequence AB128049 (Shiina et al. 2006), and cynomolgus macaque CDS sequences from the IPD-MHC NHP release 3.2.0.0 (Maccari et al. 2017). Exonerate results for each sequence list were filtered to matches of >95%, and those annotation tracks were loaded onto the polished cy0333 sequence scaffold in Geneious Prime. Annotations were manually examined and curated to retain only a single gene annotation per locus, plus CDS, ncRNA, and exon annotations as appropriate. All annotated genes were individually compared against all available human and rhesus macaque orthologs to confirm a proper annotation. In the absence of any transcription data, gene and CDS annotations spanned from start codon to stop codon for presumed transcribed genes and corresponded to human and rhesus macaque gene annotations for pseudogenes and noncoding RNAs. Gene names were assigned based on human and rhesus macaque orthologs.

### Figure generation

Gene, pseudogene, and ncRNA annotations were created from GFF3 files exported from Geneious Prime. Genomic annotation maps were generated from exported GFF3 files using the karyoploteR package (Gel and Serra 2017) and RStudio (RStudio Team 2022; <https://www.posit.co>). Additional formatting and editing to improve the readability of gene symbols were performed using Adobe Illustrator.

### Oxford Nanopore-based whole-genome reference

Although this report focuses on the full genomic MHC region, there was no feasible and economical way to sequence ultralong reads corresponding to just the MHC selectively. Therefore, we sequenced the full cy0333 MCM genome with ultralong ONT reads. *Macaca fascicularis*\_6.0 (GCA\_011100615) was generated from ~53.6× genome coverage ONT reads with corresponding Bionano optical mapping for assembly guidance. A well-characterized full genomic MHC region along with a similarly detailed full genomic KIR gene region is included within that *Macaca fascicularis*\_6.0 assembly. That assembly was error-corrected with Illumina short-read data, so accuracy is not as high as the full genomic region MHC hybrid ONT and PacBio assembly presented here (OP204634).

### Data access

All raw and processed sequencing data generated in this study have been submitted to the National Center for Biotechnology Information (NCBI; <https://www.ncbi.nlm.nih.gov/>). The raw whole-genome ONT data and raw whole-genome PacBio HiFi data have been submitted to the NCBI Sequence Read Archive (SRA; <https://www.ncbi.nlm.nih.gov/sra/>) under accession numbers SRX15982296 and SRX15982297, respectively. The final hybrid assembled ~5.2-Mb MHC genomic sequence has been submitted to the NCBI GenBank database (<https://www.ncbi.nlm.nih.gov/nucleotide/>) under accession number OP204634. Individual classical and nonclassical MHC-I and MHC-II genes have been submitted to GenBank (<https://www.ncbi.nlm.nih.gov/nucleotide/>) under accession numbers MW679584–MW679656 and ON736434–ON736437 and are listed in Supplemental Table S2. All scripts are available from the University of Wisconsin–Madison (<https://go.wisc.edu/svvlra>) and as Supplemental Scripts.

### Competing interest statement

The authors declare no competing interests.

### Acknowledgments

We thank Miranda Stauss for assistance with PacBio MHC amplicon analysis and Nicholas Minor for assistance with karyoploteR and RStudio. We also thank the expert assistance of Natasja de Groot in providing the official IPD-MHC NHP allele nomenclature for the MHC-I and MHC-II alleles reported here. We also thank R. Alan Harris, Muthuswamy Raveendran, and Jeffrey Rogers for their whole-genome assembly efforts to generate *Macaca fascicularis*\_6.0. We thank the anonymous reviewers for their careful consideration of our work and their suggestions to improve the content of this manuscript. This work was supported through contracts HHSN272201600007C and 75N93021C00006 from the National Institute of Allergy and Infectious Diseases of the National Institutes of Health. We used the University of Wisconsin–Madison Biotechnology Center's DNA Sequencing Facility (research resource identifier RRID:SCR\_017759) to generate and sequence PacBio Sequel II HiFi libraries. This work was also partly supported by the Office of Research Infrastructure Programs P51OD011106 awarded to the Wisconsin National Primate Research Center at the University of Wisconsin–Madison, and conducted in part at a facility constructed with support from Research Facilities Improvement Program grants RR15459-01 and RR020141-01.

### References

- Adams EJ, Parham P. 2001. Species-specific evolution of MHC class I genes in the higher primates. *Immunol Rev* **183**: 41–64. doi:10.1034/j.1600-065x.2001.1830104.x
- Anderson DJ, Kirk AD. 2013. Primate models in organ transplantation. *Cold Spring Harb Perspect Med* **3**: a015503. doi:10.1101/cshperspect.a015503
- Anderson JL, Sandstrom K, Smith WR, Wetzel M, Klenchin VA, Evans DT. 2022. MHC class I ligands of rhesus macaque killer-cell immunoglobulin-like receptors. bioRxiv doi:10.1101/2022.05.25.493479
- Boegel S, Löwer M, Bukur T, Sorn P, Castle JC, Sahin U. 2018. HLA and proteasome expression body map. *BMC Med Genomics* **11**: 36. doi:10.1186/s12920-018-0354-x
- Boyson JE, Iwanaga KK, Urvater JA, Hughes AL, Golos TG, Watkins DI. 1999. Evolution of a new nonclassical MHC class I locus in two Old World primate species. *Immunogenetics* **49**: 86–98. doi:10.1007/s002510050467
- Brochu H, Wang R, Tollison T, Pyo C-W, Thomas A, Tseng E, Law L, Picker LJ, Gale M Jr, Geraghty DE, et al. 2022. Alternative splicing and genetic variation of mhc-e: implications for rhesus cytomegalovirus-based vaccines. *Commun Biol* **5**: 1387. doi:10.1038/s42003-022-04344-2
- Bruijnesteijn J, van der Wiel M, de Groot NG, Bontrop RE. 2021. Rapid characterization of complex killer cell immunoglobulin-like receptor (KIR) regions using Cas9 enrichment and nanopore sequencing. *Front Immunol* **12**: 722181. doi:10.3389/fimmu.2021.722181
- Budde ML, Wiseman RW, Karl JA, Hanczaruk B, Simen BB, O'Connor DH. 2010. Characterization of Mauritian cynomolgus macaque major histocompatibility complex class I haplotypes by high-resolution pyrosequencing. *Immunogenetics* **62**: 773–780. doi:10.1007/s00251-010-0481-9
- Budde ML, Lhost JJ, Burwitz BJ, Becker EA, Burns CM, O'Connor SL, Karl JA, Wiseman RW, Bimber BN, Zhang GL, et al. 2011. Transcriptionally abundant major histocompatibility complex class I alleles are fundamental to nonhuman primate simian immunodeficiency virus-specific CD8<sup>+</sup> T cell responses. *J Virol* **85**: 3250–3261. doi:10.1128/JVI.02355-10
- Burwitz BJ, Wu HL, Abdulhaqq S, Shriver-Munsch C, Swanson T, Legasse AW, Hammond KB, Junell SL, Reed JS, Bimber BN, et al. 2017. Allogeneic stem cell transplantation in fully MHC-matched Mauritian cynomolgus macaques recapitulates diverse human clinical outcomes. *Nat Commun* **8**: 1418. doi:10.1038/s41467-017-01631-z
- Daza-Vamenta R, Glusman G, Rowen L, Guthrie B, Geraghty DE. 2004. Genetic divergence of the rhesus macaque major histocompatibility complex. *Genome Res* **14**: 1501–1515. doi:10.1101/gr.2134504
- de Groot NG, Blokhuis JH, Otting N, Doxiadis GGM, Bontrop RE. 2015. Co-evolution of the MHC class I and KIR gene families in rhesus macaques: ancestry and plasticity. *Immunol Rev* **267**: 228–245. doi:10.1111/imr.12313
- de Groot NG, Heijmans CMC, de Ru AH, Janssen GMC, Drijfhout JW, Otting N, Vangenot C, Doxiadis GGM, Koning F, van Veelen PA, et al. 2017. A specialist macaque MHC class I molecule with HLA-B\*27-like

- peptide-binding characteristics. *J Immunol* **199**: 3679–3690. doi:10.4049/jimmunol.1700502
- de Groot NG, Otting N, Maccari G, Robinson J, Hammond JA, Blancher A, Lafont BAP, Guethlein LA, Wroblewski EE, Marsh SGE, et al. 2020. Nomenclature report 2019: major histocompatibility complex genes and alleles of Great and Small Ape and Old and New World monkey species. *Immunogenetics* **72**: 25–36. doi:10.1007/s00251-019-01132-x
- de Groot NG, de Groot N, de Vos-Rouweler AJM, Louwerse A, Bruijnesteijn J, Bontrop RE. 2022. Dynamic evolution of *Mhc* haplotypes in cynomolgus macaques of different geographic origins. *Immunogenetics* **74**: 409–429. doi:10.1007/s00251-021-01249-y
- Di Genova A, Buena-Atienza E, Ossowski S, Sagot M-F. 2021. Efficient hybrid de novo assembly of human genomes with WENGAN. *Nat Biotechnol* **39**: 422–430. doi:10.1038/s41587-020-00747-w
- Doxiadis GGM, de Groot N, Otting N, de Vos-Rouweler AJM, Bolijn MJ, Heijmans CMC, de Groot NG, van der Wiel MKH, Remarque EJ, Vangenot C, et al. 2013. Haplotype diversity generated by ancient recombination-like events in the MHC of Indian rhesus macaques. *Immunogenetics* **65**: 569–584. doi:10.1007/s00251-013-0707-8
- D'Souza SS, Kumar A, Maufort J, Weinfurter JT, Raymond M, Strelchenko NS, Perrin E, Coonen J, Mejia A, Simmons HA, et al. 2022. Assessment of safety and immunogenicity of MHC homozygous iPSC-derived CD34<sup>+</sup> hematopoietic progenitors in an NHP model. *Blood Adv* **6**: 5267–5278. doi:10.1182/bloodadvances.2022006984
- Ericson AJ, Starrett GJ, Greene JM, Lauck M, Raveendran M, Deiros DR, Mohns MS, Vince N, Cain BT, Pham NH, et al. 2014. Whole genome sequencing of SIV-infected macaques identifies candidate loci that may contribute to host control of virus replication. *Genome Biol* **15**: 478. doi:10.1186/s13059-014-0478-z
- Fukami-Kobayashi K, Shiina T, Anzai T, Sano K, Yamazaki M, Inoko H, Tateno Y. 2005. Genetic evolution of MHC class I region in primates. *Proc Natl Acad Sci* **102**: 9230–9234. doi:10.1073/pnas.0500770102
- Gel B, Serra E. 2017. karyoploteR: an R/Bioconductor package to plot customizable genomes displaying arbitrary data. *Bioinformatics* **33**: 3088–3090. doi:10.1093/bioinformatics/btx346
- Greene JM, Wiseman RW, Lank SM, Bimber BN, Karl JA, Burwitz BJ, Lhost JJ, Hawkins OE, Kunstman KJ, Broman KW, et al. 2011. Differential MHC class I expression in distinct leukocyte subsets. *BMC Immunol* **12**: 39. doi:10.1186/1471-2172-12-39
- Gumá M, Angulo A, Vilches C, Gómez-Lozano N, Malats N, López-Botet M. 2004. Imprint of human cytomegalovirus infection on the NK cell receptor repertoire. *Blood* **104**: 3664–3671. doi:10.1182/blood-2004-05-2058
- Hansen SG, Ford JC, Lewis MS, Ventura AB, Hughes CM, Coyne-Johnson L, Whizin N, Oswald K, Shoemaker R, Swanson T, et al. 2011. Profound early control of highly pathogenic SIV by an effector memory T-cell vaccine. *Nature* **473**: 523–527. doi:10.1038/nature10003
- Hansen SG, Piatak M Jr, Ventura AB, Hughes CM, Gilbride RM, Ford JC, Oswald K, Shoemaker R, Li Y, Lewis MS, et al. 2013. Immune clearance of highly pathogenic SIV infection. *Nature* **502**: 100–104. doi:10.1038/nature12519
- Horton R, Wilming L, Rand V, Lovering RC, Bruford EA, Khodiyar VK, Lush MJ, Povey S, Talbot CC Jr, Wright MW, et al. 2004. Gene map of the extended human MHC. *Nat Rev Genet* **5**: 889–899. doi:10.1038/nrg1489
- Jain M, Koren S, Miga KH, Quick J, Rand AC, Sasani TA, Tyson JR, Beggs AD, Dilthey AT, Fiddes IT, et al. 2018. Nanopore sequencing and assembly of a human genome with ultra-long reads. *Nat Biotechnol* **36**: 338–345. doi:10.1038/nbt.4060
- Jayakumar V, Nishimura O, Kadota M, Hirose N, Sano H, Murakawa Y, Yamamoto Y, Nakaya M, Tsukiyama T, Seita Y, et al. 2021. Chromosomal-scale de novo genome assemblies of Cynomolgus Macaque and Common Marmoset. *Sci Data* **8**: 159. doi:10.1038/s41597-021-00935-6
- Kansler ER, Li MO. 2019. Innate lymphocytes—lineage, localization and timing of differentiation. *Cell Mol Immunol* **16**: 627–633. doi:10.1038/s41423-019-0211-7
- Karl JA, Bohn PS, Wiseman RW, Nimityongskul FA, Lank SM, Starrett GJ, O'Connor DH. 2013. Major histocompatibility complex class I haplotype diversity in Chinese rhesus macaques. *G3* **3**: 1195–1201. doi:10.1534/g3.113.006254
- Karl JA, Graham ME, Wiseman RW, Heimbruch KE, Gieger SM, Doxiadis GGM, Bontrop RE, O'Connor DH. 2017. Major histocompatibility complex haplotyping and long-amplicon allele discovery in cynomolgus macaques from Chinese breeding facilities. *Immunogenetics* **69**: 211–229. doi:10.1007/s00251-017-0969-7
- Knechtle SJ, Shaw JM, Hering BJ, Kraemer K, Madsen JC. 2019. Translational impact of NIH-funded nonhuman primate research in transplantation. *Sci Transl Med* **11**: eaau0143. doi:10.1126/scitranslmed.aau0143
- Kolmogorov M, Yuan J, Lin Y, Pevzner PA. 2019. Assembly of long, error-prone reads using repeat graphs. *Nat Biotechnol* **37**: 540–546. doi:10.1038/s41587-019-0072-8
- Koren S, Walenz BP, Berlin K, Miller JR, Bergman NH, Phillippy AM. 2017. Canu: scalable and accurate long-read assembly via adaptive *k*-mer weighting and repeat separation. *Genome Res* **27**: 722–736. doi:10.1101/gr.215087.116
- Li H. 2018. Minimap2: pairwise alignment for nucleotide sequences. *Bioinformatics* **34**: 3094–3100. doi:10.1093/bioinformatics/bty191
- Li H, Handsaker B, Wysoker A, Fennell T, Ruan J, Homer N, Marth G, Abecasis G, Durbin R, 1000 Genome Project Data Processing Subgroup. 2009. The Sequence Alignment/Map format and SAMtools. *Bioinformatics* **25**: 2078–2079. doi:10.1093/bioinformatics/btp352
- Li N, Zhang J, Liao D, Yang L, Wang Y, Hou S. 2017. Association between *C4*, *C4A*, and *C4B* copy number variations and susceptibility to autoimmune diseases: a meta-analysis. *Sci Rep* **7**: 42628. doi:10.1038/srep42628
- Loffredo JT, Sidney J, Bean AT, Beal DR, Bardet W, Wahl A, Hawkins OE, Piaskowski S, Wilson NA, Hildebrand WH, et al. 2009. Two MHC class I molecules associated with elite control of immunodeficiency virus replication, Mamu-B\*08 and HLA-B\*2705, bind peptides with sequence similarity. *J Immunol* **182**: 7763–7775. doi:10.4049/jimmunol.0900111
- Maccari G, Robinson J, Ballingall K, Guethlein LA, Grimholt U, Kaufman J, Ho C-S, de Groot NG, Flicek P, Bontrop RE, et al. 2017. IPD-MHC 2.0: an improved inter-species database for the study of the major histocompatibility complex. *Nucleic Acids Res* **45**: D860–D864. doi:10.1093/nar/gkw1050
- Malouli D, Hansen SG, Hancock MH, Hughes CM, Ford JC, Gilbride RM, Ventura AB, Morrow D, Randall KT, Taher H, et al. 2021. Cytomegaloviral determinants of CD8<sup>+</sup> T cell programming and RhCMV/SIV vaccine efficacy. *Sci Immunol* **6**: eabg5413. doi:10.1126/sciimmunol.abg5413
- Nicholas RE, Sandstrom K, Anderson JL, Smith WR, Wetzal M, Banerjee P, Janaka SK, Evans DT. 2022. KIR3DL05 and KIR3DS02 recognition of a nonclassical MHC class I molecule in the rhesus macaque implicated in pregnancy success. *Front Immunol* **13**: 841136. doi:10.3389/fimmu.2022.841136
- Norman PJ, Norberg SJ, Guethlein LA, Nemat-Gorgani N, Royce T, Wroblewski EE, Dunn T, Mann T, Alicata C, Hollenbach JA, et al. 2017. Sequences of 95 human MHC haplotypes reveal extreme coding variation in genes other than highly polymorphic *HLA class I and II*. *Genome Res* **27**: 813–823. doi:10.1101/gr.213538.116
- Nurk S, Walenz BP, Rhie A, Vollger MR, Logsdon GA, Grothe R, Miga KH, Eichler EE, Phillippy AM, Koren S. 2020. HiCanu: accurate assembly of segmental duplications, satellites, and allelic variants from high-fidelity long reads. *Genome Res* **30**: 1291–1305. doi:10.1101/gr.263566.120
- Nurk S, Koren S, Rhie A, Rautiainen M, Bizkadze AV, Mikheenko A, Vollger MR, Altemose N, Uralsky L, Gershman A, et al. 2022. The complete sequence of a human genome. *Science* **376**: 44–53. doi:10.1126/science.abj6987
- O'Connor SL, Lhost JJ, Becker EA, Detmer AM, Johnson RC, Macnair CE, Wiseman RW, Karl JA, Greene JM, Burwitz BJ, et al. 2010. MHC heterozygote advantage in simian immunodeficiency virus-infected Mauritian cynomolgus macaques. *Sci Transl Med* **2**: 22ra18. doi:10.1126/scitranslmed.3000524
- Otting N, Heijmans CMC, Noort RC, de Groot NG, Doxiadis GGM, van Rood JJ, Watkins DI, Bontrop RE. 2005. Unparalleled complexity of the MHC class I region in rhesus macaques. *Proc Natl Acad Sci* **102**: 1626–1631. doi:10.1073/pnas.0409084102
- Otting N, de Vos-Rouweler AJM, Heijmans CMC, de Groot NG, Doxiadis GGM, Bontrop RE. 2007. MHC class I A region diversity and polymorphism in macaque species. *Immunogenetics* **59**: 367–375. doi:10.1007/s00251-007-0201-2
- Rölle A, Pollmann J, Ewen E-M, Le VTK, Halenius A, Hengel H, Cerwenka A. 2014. IL-12-producing monocytes and HLA-E control HCMV-driven NKG2C<sup>+</sup> NK cell expansion. *J Clin Invest* **124**: 5305–5316. doi:10.1172/JCI77440
- Rosner C, Kruse PH, Lübke T, Walter L. 2010. Rhesus macaque MHC class I molecules show differential subcellular localizations. *Immunogenetics* **62**: 149–158. doi:10.1007/s00251-010-0424-5
- RStudio Team. 2022. *RStudio: integrated development for R*. Posit Software, PBC, Boston. <https://www.posit.co>.
- Shiina T, Blancher A. 2019. The cynomolgus macaque MHC polymorphism in experimental medicine. *Cells* **8**: 978. doi:10.3390/cells8090978
- Shiina T, Ota M, Shimizu S, Katsuyama Y, Hashimoto N, Takasu M, Anzai T, Kulski JK, Kikkawa E, Naruse T, et al. 2006. Rapid evolution of major histocompatibility complex class I genes in primates generates new disease alleles in humans via hitchhiking diversity. *Genetics* **173**: 1555–1570. doi:10.1534/genetics.106.057034
- Shiina T, Blancher A, Inoko H, Kulski JK. 2017. Comparative genomics of the human, macaque and mouse major histocompatibility complex. *Immunology* **150**: 127–138. doi:10.1111/imm.12624
- Shortreed CG, Wiseman RW, Karl JA, Bussan H, Baker DA, Prall TM, Haj AK, Moreno GK, Penedo MCT, O'Connor DH. 2020. Characterization

- of 100 extended major histocompatibility complex haplotypes in Indonesian cynomolgus macaques. *Immunogenetics* **72**: 225–239. doi:10.1007/s00251-020-01159-5
- Sun JC, Beilke JN, Lanier LL. 2009. Adaptive immune features of natural killer cells. *Nature* **457**: 557–561. doi:10.1038/nature07665
- Sussman RW, Tattersall I. 1986. Distribution, abundance, and putative ecological strategy of *Macaca fascicularis* on the Island of Mauritius, southwestern Indian ocean. *Folia Primatol* **46**: 28–43. doi:10.1159/000156234
- Tomasec P, Braud VM, Rickards C, Powell MB, McSharry BP, Gadola S, Cerundolo V, Borysiewicz LK, McMichael AJ, Wilkinson GW. 2000. Surface expression of HLA-E, an inhibitor of natural killer cells, enhanced by human cytomegalovirus gpUL40. *Science* **287**: 1031–1033. doi:10.1126/science.287.5455.1031
- Trowsdale J, Knight JC. 2013. Major histocompatibility complex genomics and human disease. *Annu Rev Genomics Hum Genet* **14**: 301–323. doi:10.1146/annurev-genom-091212-153455
- Voogd L, Ruijbal P, Ottenhoff THM, Joosten SA. 2022. Antigen presentation by MHC-E: a putative target for vaccination? *Trends Immunol* **43**: 355–365. doi:10.1016/j.it.2022.03.002
- Warren WC, Harris RA, Haukness M, Fiddes IT, Murali SC, Fernandes J, Dishuck PC, Storer JM, Raveendran M, Hillier LW, et al. 2020. Sequence diversity analyses of an improved rhesus macaque genome enhance its biomedical utility. *Science* **370**: eabc6617. doi:10.1126/science.abc6617
- Watanabe A, Shiina T, Shimizu S, Hosomichi K, Yanagiya K, Kita YF, Kimura T, Soeda E, Torii R, Ogasawara K, et al. 2007. A BAC-based contig map of the cynomolgus macaque (*Macaca fascicularis*) major histocompatibility complex genomic region. *Genomics* **89**: 402–412. doi:10.1016/j.ygeno.2006.11.002
- Weatherall D. 2006. The use of non-human primates in research. *The National Archives*. NHP Study Working Group, London. <https://webarchive.nationalarchives.gov.uk/ukgwa/20220207162925/http://mrc.ukri.org/documents/pdf/the-use-of-non-human-primates-in-research/> [accessed July 12, 2022].
- Wenger AM, Peluso P, Rowell WJ, Chang P-C, Hall RJ, Concepcion GT, Ebler J, Fungtammasan A, Kolesnikov A, Olson ND, et al. 2019. Accurate circular consensus long-read sequencing improves variant detection and assembly of a human genome. *Nat Biotechnol* **37**: 1155–1162. doi:10.1038/s41587-019-0217-9
- Wiseman RW, Karl JA, Bohn PS, Nimityongskul FA, Starrett GJ, O'Connor DH. 2013. Haplessly hoping: macaque major histocompatibility complex made easy. *ILAR J* **54**: 196–210. doi:10.1093/ilar/ilt036
- Wu HL, Wiseman RW, Hughes CM, Webb GM, Abdulhaqq SA, Bimber BN, Hammond KB, Reed JS, Gao L, Burwitz BJ, et al. 2018. The role of MHC-E in T cell immunity is conserved among humans, rhesus macaques, and cynomolgus macaques. *J Immunol* **200**: 49–60. doi:10.4049/jimmunol.1700841
- Yang Y, Chung EK, Wu YL, Savelli SL, Nagaraja HN, Zhou B, Hebert M, Jones KN, Shu Y, Kitzmiller K, et al. 2007. Gene copy-number variation and associated polymorphisms of complement component C4 in human systemic lupus erythematosus (SLE): low copy number is a risk factor for and high copy number is a protective factor against SLE susceptibility in European Americans. *Am J Hum Genet* **80**: 1037–1054. doi:10.1086/518257

Received October 24, 2022; accepted in revised form February 21, 2023.